Surface-dependent activity of model CoMoS hydrotreating catalysts

Ricardo Garcia de Castro, Elodie Devers, Mathieu Digne, Anne-Félicie Lamic-Humblot, Gerhard Pirngruber, Xavier Carrier

Surface-dependent activity of model CoMoS hydrotreating catalysts

Ricardo GARCIA DE CASTRO,[1,2] Elodie DEVERS,[2] Mathieu DIGNE,[2] Anne-Félicie LAMIC-HUMBLOT,[1] Gerhard D. PIRNGRUBER,[2] Xavier CARRIER[1,*]

1- Sorbonne Université, CNRS, Laboratoire de Réactivité de Surface, 75005 Paris (France)

2- IFP Energies nouvelles, Rond-point de l'échangeur de Solaize, 69360 Solaize (France)

*xavier.carrier@sorbonne-universite.fr

Abstract

The current environmental and industrial contexts require constant revision and improvement of hydrotreating processes for obtaining cleaner (bio)fuels through the development of supported transition metal sulfide (TMS) catalysts. The present work proposes a surface-science approach to describe the surface-dependent genesis of the cobalt-promoted active phase (CoMoS) supported on α-Al_2O_3 single crystals used as surrogates of the industrial γ-Al_2O_3 support. Co-Mo precursor solutions are deposited by aqueous-phase impregnation onto four α-Al_2O_3 single crystals of C(0001), A(11$\bar{2}$0), M(10$\bar{1}$0), and R(1$\bar{1}$02) orientations, which display specific OH sorption sites. The model catalysts are characterized in the oxide and sulfide states by XPS, AFM, and TEM revealing a surface dependent sulfidation and dispersion as a result of metal-support interactions of diverse nature. The surfaces can be ranked following metal-support interactions of increasing strength C(0001)< A(11$\bar{2}$0), M(10$\bar{1}$0) < R(1$\bar{1}$02) in good agreement with model non-promoted catalysts. However, AFM and TEM imaging also reveal that cobalt incorporation leads to an increase in the stacking of CoMoS particles with respect to non-promoted catalysts. The activity of the model catalysts in thiophene hydrodesulfurization cannot be simply related to the common features of the active phase (sulfidation, dispersion, promotion extent) but a volcano-shape curve is obtained when plotting the activity as a function of metal-support interactions. These results suggest that high activity is obtained on surfaces with intermediate metal-support interactions that lead to an optimal metal-sulfur bond energy in agreement with the Sabatier principle. Transposing these results to the traditional γ-Al_2O_3 support suggests an enhanced activity of the (100) facet, which can lead to the development of improved supports for hydrotreating catalysts.

1. Introduction

Hydrotreating has been an essential step in crude oil refineries for decades due to their role in the elimination of heteroatoms (e.g. sulfur, nitrogen, oxygen and heavy metals) from petroleum feedstocks. More recently, hydrotreating for deoxygenation of biofuels is in increasing demand for upgrading the quality of pyrolysis oils from second generation biomass [1]. Hydrotreating is carried out via heterogeneous catalysis using highly-dispersed, γ-Al_2O_3-supported promoted transition metal sulfides (TMS, e.g. CoMo) [2–6]. Several decades of continuous improvement of the reaction conditions and the catalyst itself have progressively increased the efficiency of the hydrotreating process in order to meet ever-tightening environmental requirements [7]. However, the development of more efficient hydrotreating catalysts is now driven not only by a reduction in heteroatom emissions but also by improving the atom economy in order to be fully aligned with industrial sustainability. Such a fine-tuning of catalyst activity necessarily calls for a more rational catalyst formulation through molecular design.

Starting from the 1980s, the advent of finer characterization techniques (Mössbauer, XPS, XAS) allowed obtaining a clear picture of the nature of supported hydrotreating catalysts: hexagonal-like MoS_2 lamellar structures dispersed on γ-Al_2O_3, with cobalt decorating their edges. The active phase (commonly referred to as CoMoS phase) has been thoroughly characterized since its model was first proposed by Topsøe et al. [6,8,9] From a 2D geometric model of the MoS_2 slab [5] to DFT calculations detailing the chemistry of the CoMoS edges [10,11], extensive research of the active phase at the molecular level has allowed to improve catalyst formulations up to its current standards. However, the nature of the active phase-support interactions yet remains a key point that has not been fully resolved, especially at the molecular scale. The polycrystalline nature of γ-Al_2O_3 nanoparticles leads to a variety of surface sorption sites (-OH groups) that renders a detailed study of their interactions with the active phase challenging. A molecular-scale description of these interactions could allow us to correlate active phase properties such as dispersion, sulfidation degree, and catalytic activity to specific surface sorption sites present on the support. Since traditional polycrystalline supports are not able to provide controlled surface speciation, a surface-science approach that uses single crystals as supports can be used instead. This reductionist approach has proven to be a fruitful alternative for the study of hydrotreating catalysts. For instance, Lauritsen et al. [12–15] studied the growth of single and multi-layered MoS_2 and CoMoS slabs on metallic single crystals (Au(111)) via STEM. Muijsers et al. [16] studied the sulfidation of Mo oxides on planar SiO_2/Si(100). Sakashita et al. [17,18] prepared γ-Al_2O_3 thin films on a Mg-Al spinel substrate with controlled surface orientations. This latter study used transmission electron microscopy to show that some properties like orientation of the active phase (with respect to the support) and stacking number were related to the alumina crystal plane. More recently, Bara et al. [19] reviewed the importance of surface-science approaches to gain insight into the role of different alumina surface orientations on the properties of hydrotreating catalysts. From this, a reductionist strategy using commercially available α-Al_2O_3 single crystals of different surface orientations as supports was developed. Single crystals of A$(11\bar{2}0)$, C(0001), M$(10\bar{1}0)$, and R$(1\bar{1}02)$ α-Al_2O_3 orientations were used as model planar supports since they provide well defined surface -OH speciation. These surface hydroxyl groups can then be compared to those found on the different facets of γ-Al_2O_3 in order to establish a parallelism between the sites from both materials and therefore allow the use of model α-Al_2O_3 surfaces as surrogates for the study of traditional hydrotreating catalysts since the speciation of surface -OH groups on both materials has been the subject of extensive experimental and theoretical research. This parallelism has been reviewed before [19–22] even if one has to be aware that the surface structure of γ-Al_2O_3 is still highly discussed in the literature [23]. Bara et al. [20,21] successfully implemented this approach for non-promoted Mo-based catalysts using the aforementioned α-Al_2O_3 planar supports. Moreover, this model approach sought to mimic incipient wetness impregnation for precursor deposition on the planar surfaces in order to be closer to industrial synthesis conditions. In that sense, aqueous-phase preparation on model alumina wafers served as an alternative to the typical surface-science preparation methods (e.g. ultra-high vacuum), allowing to narrow the gap between model systems and commercial catalysts. The studies concluded that parameters such as sulfidation degree, dispersion, and orientation of MoS_2 slabs relative to the support are surface-dependent, in close agreement with Sakashita et al. [17,18], and established that these parameters are governed by the strength of metal-support interactions.

This work aims at taking a step further into bridging the material gap by preparing cobalt-promoted catalysts using the surface-science approach described above. A further challenge is to link the surface-dependent active phase structures and their catalytic properties, which was not possible for non-promoted systems due to their very low intrinsic activity. For that, Co-promoted Mo/α-Al_2O_3 model catalysts supported on α-Al_2O_3 planes A$(11\bar{2}0)$, C(0001), M$(10\bar{1}0)$, and R$(1\bar{1}02)$ were synthesized by aqueous-phase deposition. The model catalysts were studied in the oxide and sulfide states by XPS (sulfidation of slabs, edge decoration by promoter) and AFM (dispersion), while TEM was used to evaluate the size and stacking of CoMoS slabs. Finally, the model

catalysts were tested in a model thiophene hydrodesulfurization reaction in order to relate the active phase properties with its intrinsic catalytic activity.

2. Materials and Methods

2.1 Preparation of model Co-Mo/α-Al_2O_3 catalysts

Model HDS catalysts were prepared on planar α-Al_2O_3 squared-single crystals (wafers) with four crystal orientations. A$(11\bar{2}0)$ and R$(1\bar{1}02)$ plane wafers were purchased from MaTecK Material Technologie & Kristalle GmbH (Germany). C(0001) and M$(10\bar{1}0)$ wafers were provided by SurfaceNet GmbH (Germany). The wafers had dimensions of 1.0 cm x 1.0 cm x 0.50 mm (thickness), which corresponds to an available surface area of 1.0 cm^2 per wafer.

The wafers were chemically cleaned before precursor solution deposition. The cleaning methodology was directly adopted from the procedure established by the work of Tougerti et al. [24], consisting of the following rinsing steps: 25 mL of distilled water (30 min), 25 mL HNO_3 (30 min, pH 2), 25 mL of distilled water (30 min), 25 mL of NH_4OH (30 min, pH 9), 25 mL of distilled water (30 min). The rinsing steps were carried out by a synthesis robot (Zinsser Analytic). After the washing procedure was completed, the wafers were dried under a nitrogen flux and posteriorly calcined at 700 °C for 14 h, using an ascending temperature ramp of 6 °C/min in air inside a muffle furnace.

The Co-Mo-based model catalysts in this work were synthesized by co-impregnation of Co and Mo metal salts through deposition of 100 µL of aqueous precursor solution. The solution was prepared with a Co/Mo molar ratio of 0.5 [25,26]. The metal salt precursors were ammonium heptamolybdate (AHM), $(NH_4)_6Mo_7O_{24}$, and cobalt nitrate, $Co(NO_3)_2$. The concentration of the precursor solutions was $6.8 \cdot 10^{-6}$ mol.L^{-1} in Mo and $3.4 \cdot 10^{-6}$ mol.L^{-1} in Co, in order to ensure a surface concentration of ~ 4.0 atoms·nm^{-2} in molybdenum and ~ 2.0 atoms·nm^{-2} in cobalt. These loadings would correspond to ~16 wt% MoO_3 and ~5 wt% CoO for a traditional 200 $m^2 \cdot g^{-1}$ γ-Al_2O_3 powder support. Precursor solution deposition (drop-casting) was carried out with an Eppendorf pipette that allowed the 100 µL solution to cover the entire surface of the crystal. After deposition, the wafers were dried under vacuum for 1 h and then calcined for 2 h at 450 °C using an ascending temperature ramp of 6 °C/min in air inside a muffle furnace.

2.2 Sulfidation of model catalysts

The model catalysts were sulfided (activated) in a glass reaction cell (≈ 27 mL). The sulfidation scheme proceeded as follows: first, the system was purged with 2NL·h^{-1} argon flow for five minutes. Gas phase sulfidation commenced at atmospheric pressure under a 2NL·h^{-1} 15% mol H_2S/H_2 gas flow before heating the sulfidation cell at 5 °C/min until reaching the target temperature (100, 200, 300, 400, or 500 °C). This temperature was kept constant for 2 h before switching to Ar at 2NL·h^{-1} and cooling down in a 15 °C/min descending ramp up to 150°C (or 80 °C for sulfidation at 100 °C). Subsequently, the argon atmosphere was kept at this temperature for 1 h. Finally, the system reached ambient temperature under argon flux. After the sulfidation cycle was completed, the activated catalysts were kept under argon atmosphere inside a hermetic storage device.

2.3 Characterization of model catalysts

2.3.1 X-ray photoelectron spectroscopy

XPS spectra were obtained with an Omicron (ESCA+) instrument using a monochromatic Al X-ray source (hv = 1486.6 eV) with an accelerating voltage of 14 kV and a current of 20 mA (with an overall energy resolution of 0.8 eV). The spectra were collected at a takeoff angle of 90° under a pressure below $1 \cdot 10^{-9}$ mbar at ambient temperature. In order to obtain high-resolution spectra, the analyzer operated at an energy of 20 eV for the selected elemental scanning and 100 eV for the overall elemental survey. The scans were performed using a 0.1 eV step over the selected elements. The surveyed regions were C1s, O1s, Al2p, Mo3d, Co2p, and S2p. The obtained spectra for each scanned region were calibrated based on the C1s photopeak of adventitious carbon at 284.6 eV [25,26], An electron flood-gun was required in order to ensure charge neutralization of the alumina substrate as it is an insulating material that will undergo surface charging upon ejection of the photoelectrons. After spectra collection, the mathematical decomposition of the different contributions was performed using the Casa XPS software [27]. The decomposition of

the obtained spectra was carried out using Gaussian-Lorentzian functions, while the background subtraction was Shirley-type. Spectral decomposition of the Mo3d, S2s, S2p, and Co2p regions was carried out by following the premises established by Gandubert et al. [25,26] and a standardized procedure based on a common set of binding energy and FWHM restrictions was imposed on every spectrum for the sake of consistency.

The surface density (in atoms·nm^{-2}) of molybdenum and cobalt was calculated for each planar catalyst according to the quantification model used by Tougerti et al.[24] derived from the work of Towle et al. [28]. The expression for Mo surface density (and cobalt respectively) is given by:

$$[\mathrm{Mo\ or\ Co}]_{\mathrm{surface}} = \frac{\mathrm{A_{Mo3d/Co2p}}\ \sigma_{\mathrm{Al2p}}\ 2\rho_{\mathrm{Al2O3}}}{\mathrm{A_{Al2p}}\ \sigma_{\mathrm{Mo3d\ /Co2p}}\mathrm{MW_{Al2O3}}} \cdot \lambda_{\mathrm{Al}}\ \cdot \mathrm{N_A} \qquad (1)$$

where A_{Mo3d} and A_{Al2p} are the total areas of the Mo3d (Co2p) and Al2p XPS photopeak regions, σ_{Al2p} and σ_{Mo3d} are the photoionization cross-sections (0.441 for Al, 8.19 for Mo), ρ_{Al2O3}, and MW_{Al2O3} are the density and molar mass of α-Al_2O_3 (3.95 g·cm^{-3} and 102 g·mol^{-1}). λ_{Al} is the average mean free path of Al photoelectrons in Al_2O_3 (3.28 nm [29]). N_A is the Avogadro constant. The same expression was used to calculate the Co surface density using the area of the Co2p peak and the ($\sigma_{Co2p} = 17.4$) cross section, respectively.

The Mo3d XPS spectra of sulfided Mo-based catalysts were decomposed into three contributions: MoO_3, MoO_xS_y, and MoS_2. By expressing the total Mo surface density as a sum of the areas corresponding to the three Mo contributions, the relative percentage of MoS_2 with respect to the rest of Mo species, was calculated as:

$$\%\ \mathrm{MoS_2} = \frac{\mathrm{A_{MoS_2}}}{\mathrm{A_{MoS_2}} + \mathrm{A_{MoO_xS_y}} + \mathrm{A_{MoO_3}}} \times 100 \qquad (2)$$

%MoS_2 will be referred hereto as sulfidation degree.

The Co2p XPS region was also decomposed into three contributions: Co^{2+}, Co_9S_8, and CoMoS. The relative percentage of Co incorporated at the edges of MoS_2 (CoMoS phase) on each model catalyst was calculated according to Eq. 3 and will be referred to as the promotion extent.

$$\%\ \mathrm{CoMoS} = \frac{\mathrm{A_{CoMoS}}}{\mathrm{A_{CoMoS}} + \mathrm{A_{Co_9S_8}} + \mathrm{A_{Co^{2+}}}} \times 100 \qquad (3)$$

Sample transfer from the hermetic storage recipient to the XPS chamber was carried out via a rapid procedure (less than 1 minute). It was duly verified that samples did not undergo significant re-oxidation during the transfer.

2.3.2 Atomic force microscopy (AFM)

Model catalysts studied in this work were imaged by AFM in the oxide and sulfide phases using a Nanoscope VIII Multimode AFM (Bruker, USA) through peak force tapping mode at 2 kHz resonance frequency. Every analyzed sample was imaged at two or three different locations on the surface. Height and lateral profiles were obtained from the images for each model catalyst. The probing tips were purchased from Bruker (United States). The model was a SCANASYST-AIR silicon tip on nitride lever with a force constant of 0.4 N/m.

2.3.3 Transmission electron microscopy (TEM)

Conventional TEM images were collected with a JEOL 2010 microscope operating at 200 kV. The average MoS_2 slab length and stacking number were obtained by measuring no less than 220 clusters per sample for statistical purposes, using the ImageJ 1.45 software [30]. TEM samples were prepared by scraping the surface of the wafers with a stainless-steel razor blade in order to obtain fragments of the model samples thin enough to carry out electron microscopy. The detached fragments were suspended into a drop of absolute ethanol, which was then deposited on a carbon-coated Cu-grid for TEM analysis. The slab length for each MoS_2 slab was obtained by manually measuring the visible darkened stripes that contrasted with the lighter α-Al_2O_3 background. The stacking number was determined by quantification of visible stripe layers for every MoS_2 cluster.

2.3.4 Assessment of Mo substitution by Co at MoS_2 edges

XPS and TEM results allow the quantification of the substitution of molybdenum atoms at the edges of MoS_2 by cobalt following the geometric model of MoS_2 slabs proposed by Kasztelan et al. [5] The mean Co/Mo ratio within the slabs $(Co/Mo)_{CoMoS}$ was defined as:

$$(\mathrm{Co/Mo})_{\mathrm{CoMoS}} = \frac{\text{Co loading} \times \%\mathrm{CoMoS}}{\text{Mo loading} \times \%\mathrm{MoS_2}} \qquad (4)$$

with Co and Mo loadings in atoms·nm^{-2} and %CoMoS and $\%MoS_2$ as the promotion extent and sulfidation degree, obtained by XPS respectively.

The substitution level (in %) of Co atoms was defined as:

$$\mathrm{Sub_{level}} = \frac{(\mathrm{Co/Mo})_{\mathrm{CoMoS}}}{1 + (\mathrm{Co/Mo})_{\mathrm{CoMoS}}} \times \frac{\text{Mo total}}{\text{Mo edges} + \text{corners}} \times 100\% \qquad (5)$$

The substitution level corresponds to the proportion of edges and corners sites that are occupied / substituted by a Co atom. With the total amount of Mo atoms within the slabs (Mo total) and the amount of Mo atoms on edges and corners calculated using the slab lengths obtained experimentally by TEM. The number of Mo atoms in edges, corners, and basal plane of a MoS_2 slab is deduced from the Mo-Mo distance (3.2 Å) [3] and the average slab length determined experimentally (see Fig. 8).

2.3.5 Grazing-incidence X-ray absorption spectroscopy (GI-XAS)

The planar catalysts were characterized by GI-XAS (grazing-incidence X-ray absorption spectroscopy) in fluorescence mode with a Canberra 35 elements solid-state Ge detector at the Co K edge (7.7 keV) on the SAMBA beamline at SOLEIL (Saint-Aubin, France) [31]. The model catalysts were analyzed inside a protective device in which continuous argon circulation was guaranteed in order to prevent re-oxidation of cobalt atoms. The device was designed at SOLEIL facilities, allowing the transmission of X-rays and fluorescent photons through a Kapton protective film covering the sample. The device was then mounted on a triple axis goniometer to align the sample surface parallel to the incident radiation electric field or perpendicular, while keeping the ability to rotate them and aligning at close to grazing incidence. This also ensured the analysis of the exact same location of the wafer at both polarizations. Each model catalyst was first sulfided at 300 °C and then analyzed in two polarization modes, parallel and perpendicular. Processing of the XAS data was carried out with the Demeter package [32]. The reference Co_9S_8 XAS spectrum was kindly provided by V. Briois (SOLEIL synchrotron) following a temperature-programmed method reported by Plais et al. [33].

2.4 Thiophene hydrodesulfurization

Gas-phase thiophene hydrodesulfurization was conducted in batch configuration at 400 °C for 24 h at atmospheric pressure (1 bar). The reactor used for the catalytic tests was the same as the one used for sulfidation (section 2.2). Four identical samples (single crystals) of each model catalyst, whose preparation is detailed in Section 2.1, were first placed inside the reactor and sulfided at 400 °C; then, the reactor was purged with a flow of argon for 2 h until reaching ambient temperature. Thiophene was initially introduced in the reactor as a saturated vapor in a thiophene/H_2 stream. Thiophene saturation was obtained by bubbling H_2 (flowrate 1L/h) into liquid thiophene (Sigma Aldrich) in a reservoir submerged in a temperature-controlled bath at 14.1 °C (corresponding to a vapor pressure of 2800 Pa). After flushing the reactor with the thiophene/H_2 mixture for 15 min, an initial analysis (at ambient temperature and pressure) was carried out by gas chromatography (GC) equipped with a flame ionization detector. The reactor was then heated up to 400 °C (5 °C·min^{-1} ramp from ambient temperature) before sealing it; the reaction was carried out in batch mode for 24 h. The product analysis was finally carried out at ambient temperature at the end of the reaction. Reactants were pushed towards the GC injection loop (6-way valve) with the help of a syringe pump.

The GC column allowed the identification of five products of the thiophene hydrodesulfurization reaction: n-butane, trans-2-butene, 1-butene, cis-2-butene, and 1,3-butadiene. The GC response factor (peak area/concentration in ppm) was measured for 1,3-butadiene from a 1,3-butadiene/He mixture of known concentration and then assuming identical response factors for all C4 products [34]. The response factor for thiophene was measured independently and closely matched the expected value from the number of ionizable carbon atoms.

The conversion after 24 h in batch mode was defined as:

$$X_{thiophene} = \frac{\sum_n C_i}{\sum_n C_i + C_{thiophene\ t=24h}} \qquad (6)$$

where C_i is the concentration (in ppm) of product "i" and $C_{thiophene\ t=24h}$ is the remaining thiophene concentration after 24 h of reaction. The conversion was defined from product concentration instead of the difference between the final and initial thiophene concentration due to the very low conversion which is of the order of magnitude of the error in thiophene concentration between measurements.

A TOF is difficult to estimate in the present conditions (batch mode, single crystals) due to the difficulty of reaching an accurate measurement of the volume of the glass reactor. However, a normalized conversion was determined instead in order to compare samples with respect to the amount of active sites. The conversion obtained by Eq. (6) was normalized by the number of Mo moles in edges and corners of MoS_2 slabs (active sites)

$$\varphi/(\text{mol Mo edge} + \text{corners}) = \frac{X}{\text{mole Mo} \cdot \%\ MoS_2 \cdot \overline{D}} \qquad (7)$$

where

φ = normalized conversion / $(\text{mol Mo edge} + \text{corners})^{-1}$

X = conversion

mole Mo = total number of surface Mo (mol.) determined by XPS

% MoS_2 = sulfidation degree

$\overline{D}$ = average lateral dispersion

We define the average lateral dispersion as the weighted average of individual lateral dispersion values. The weighted average is obtained by weighing individual dispersions (D_i) for a given slab length by its frequency (f_i, %) in the slab length distribution histogram (Fig. 8):

$$\overline{D} = \sum_{i=1\ nm}^{10\ nm} \frac{D_i \cdot f_i}{100} \qquad (8)$$

Individual dispersions (D_i) are defined as the fraction of Mo atoms in edge and corner positions according to the model of S. Kasztelan. [5]:

$$D_i = \frac{6n_i - 6}{3n_i^2 - 3n_i + 1} \qquad (9)$$

where n_i are the number of atoms filling up the hexagon diameter for a given slab length, according to the expression:

$$L_i = 2 \cdot n_i \cdot d \qquad (10)$$

where

L_i is the slab length

d = Mo – Mo interatomic distance determined by EXAFS (3.2 Å)

After each reaction cycle, the product selectivity was also calculated according to the following expression:

$$S_i = \frac{C_i}{\sum_i C_i} \cdot 100\% \qquad (11)$$

where S_i is the selectivity of product "i" and C_i the concentration of product "i".

3. Results

3.1 Characterization of the model catalysts in the oxide state

Five to six impregnated wafers of each crystal plane were analyzed in the oxide state (after 2 h calcination at 450 °C) by XPS in order to confront the expected metal surface density and the experimental one determined from Eq. (1) and the areas of the XPS Mo3d and Co2p photopeaks (Fig. 1).

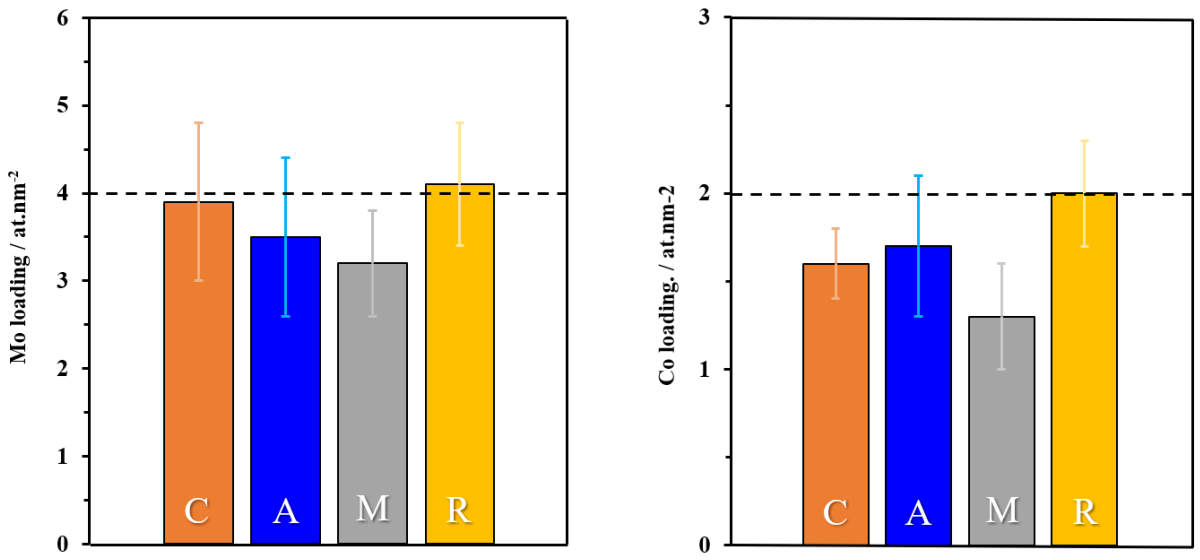

Figure 1. Average Mo and Co loadings calculated from the corresponding XPS Mo3d and Co2p areas and Eq. (1) for model Co-Mo catalysts supported on the C(0001), A$(11\bar{2}0)$, M$(10\bar{1}0)$, and R$(1\bar{1}02)$ planes of α-Al_2O_3. The dotted line represents the expected loading (4 atoms·nm^{-2} for Mo and 2 atoms·nm^{-2} for Co). The error bars are the standard deviation of 5-6 measurements made for each crystal plane.

As seen in Fig. 1, the average surface densities for both Mo and Co closely approach the expected values of 4 and 2 atoms·nm^{-2}, respectively. Nevertheless, there is a slight underestimation of the surface concentration for both atoms on the A$(11\bar{2}0)$ and M$(10\bar{1}0)$ planes and for Co on the C(0001) plane. This effect could be attributed to the presence of metal aggregates on the surface, with thickness higher than the average mean free path of Al photoelectrons. In that case, Eq. (1) which supposes no attenuation of Al photoelectrons from the alumina matrix when passing through the Mo/Co deposits is not perfectly applicable anymore [24]. However, Eq. (1) has the advantage of making no a priori assumptions concerning the overlayer morphology.

The best match between the experimental metal loadings and the expected values is found for R$(1\bar{1}02)$ plane-based catalysts, suggesting high metal dispersion in the oxide state for these model catalysts. This result is in agreement with those reported by Bara et al. [21], who showed that model Mo-based catalysts supported on the R$(1\bar{1}02)$ plane displayed well dispersed MoO_x particles. The present results confirm that MoO_x supported on the R$(1\bar{1}02)$ plane will be better dispersed than on the C(0001), A$(11\bar{2}0)$, and M$(10\bar{1}0)$ planes and suggests a better dispersion of cobalt atoms on the former support as well. The aggregation effect on XPS intensities has also been detected by a similar XPS-based method to quantify dispersion [35].

The calculated average Co/Mo ratio for each crystal plane was also confronted to its expected value and experimental results were very close to the theoretical one (0.5) and did not vary significantly from one crystal plane to another (Table 1).

Table 1. Average Co/Mo ratio for the CoMo model catalysts supported on the C(0001), A$(11\bar{2}0)$, M$(10\bar{1}0)$, and R$(1\bar{1}02)$ crystal planes of α-Al_2O_3 in the oxide state after calcination at 450°C.

Ratio	C(0001)	A$(11\bar{2}0)$	M$(10\bar{1}0)$	R$(1\bar{1}02)$
Co/Mo	0.41	0.49	0.41	0.49

Due to the planar nature of the support, atomic force microscopy (AFM) can be used to study the topography of the model catalysts in order to obtain an overview of metal repartition on the surface, despite being unable to discern between Co and Mo oxides. The images (Fig. 2) were recorded after impregnation and 450 °C calcination and then analyzed in terms of particle size and

surface roughness. Reference AFM images of clean surfaces of single crystals with A$(11\bar{2}0)$, C(0001), M$(10\bar{1}0)$, and R$(1\bar{1}02)$ orientations prior to precursor solution deposition and corresponding topographic profile are available on a previous contribution [22].

Figure 2 reveals two types of topographic profiles for model catalysts in the oxide phase. The first one is an aggregate-like profile, exhibited by catalysts supported on the A$(11\bar{2}0)$, C(0001), and M$(10\bar{1}0)$ planes. These model catalysts exhibit aggregates with average diameter ranging from 66 to 79 nm and typical heights of 5-15 nm. The second type is exhibited by R$(1\bar{1}02)$ plane-based catalysts, which display much more dispersed metal oxides, with average particle diameter of 54 nm and typical particle heights ranging from one to two nm.

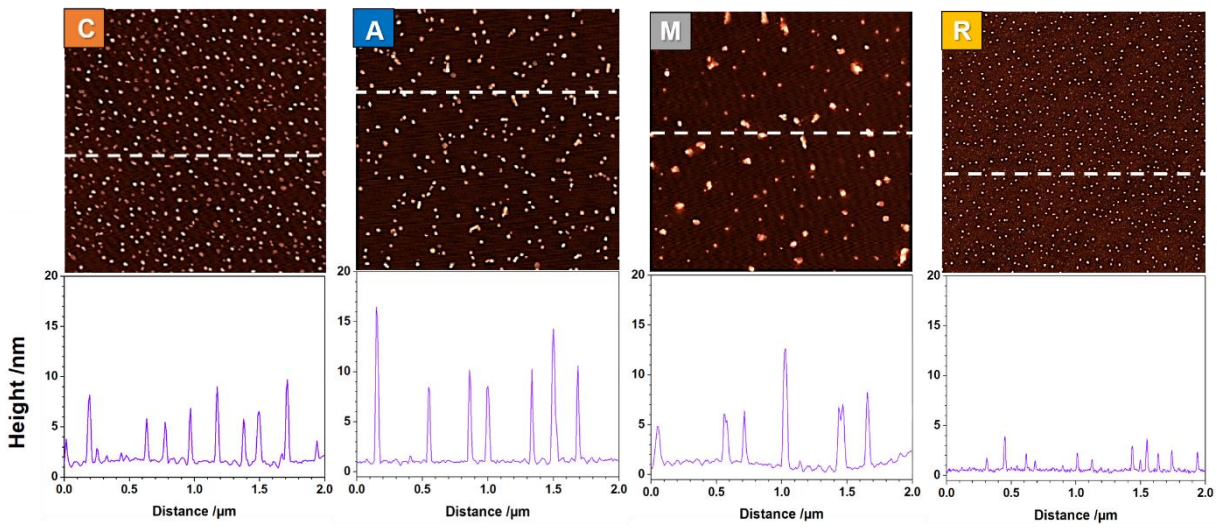

Figure 2. 2 μm x 2 μm AFM images (top) and height profiles (bottom) for series of Co-Mo-based model catalysts supported on the C(0001), A$(11\bar{2}0)$, M$(10\bar{1}0)$, and R$(1\bar{1}02)$ crystal planes of α-Al_2O_3 after calcination at 450 °C. The white dashed line represents the segment of the image from which the height profile was obtained.

The topographic profiles seen in Fig. 2 closely resemble those of non-promoted Mo/α-Al_2O_3 in the oxide phase, as these also showed aggregate-like behavior for A$(11\bar{2}0)$, C(0001), and M$(10\bar{1}0)$ plane-based catalysts and more dispersed particle-like for those supported on the R$(1\bar{1}02)$ plane [21]. This suggests that the presence of cobalt cations does not alter Mo-support interactions previously discussed. Table 2 displays the mean surface roughness of oxide CoMo/α-Al_2O_3 model catalysts supported on the A$(11\bar{2}0)$, C(0001), M$(10\bar{1}0)$, and R$(1\bar{1}02)$ crystal planes and of clean wafers of each plane as reference.

The mean roughness of single crystals of all four α-Al_2O_3 orientations (Table 2) is virtually the same prior to metal precursor deposition. After being impregnated with the precursor solution, distinctive surface roughness values emerge as a consequence of oxoanion-surface sites interactions characteristic for each crystal plane. The lowest surface roughness is reported for the R$(1\bar{1}02)$ plane-based catalyst, which exhibits visibly higher dispersion (Fig. 2), due to strong oxoanion-sorption sites interactions typical of Al_{4C}-μ_1-OH sites [20,21].

Table 2. Root mean square surface roughness (Rrms) of the clean wafers and CoMo model catalysts supported on single crystal wafers of planes C(0001), A$(11\bar{2}0)$, M$(10\bar{1}0)$, and R$(1\bar{1}02)$ of α-Al_2O_3 and calcined at 450 °C for 2 h obtained via AFM measurements at a scale of 2 μm x 2 μm. The Rrms calculation is detailed in the supporting information section. AFM images of clean wafers are available in a prior contribution [22].

Rrms /nm	C(0001)	A$(11\bar{2}0)$	M$(10\bar{1}0)$	R$(1\bar{1}02)$
Clean Wafer	0.13 ± 0.01	0.12 ± 0.01	0.12 ± 0.01	0.13 ± 0.01
Calcined catalyst	0.94 ± 0.01	0.72 ± 0.01	0.67 ± 0.01	0.48 ± 0.01

On the contrary, C(0001) plane-based catalysts exhibit poorly-dispersed aggregates, in agreement with weaker oxoanion-support interaction associated to Al_{6C}-μ_2-OH sites, the fingerprint of C(0001) plane [19,21,36]. A$(11\bar{2}0)$ and M$(10\bar{1}0)$ plane-based catalysts exhibit intermediate roughness compared to the previously discussed cases. This behavior can also be explained by the

nature of their surface terminations, constituted by Al_{6C}-$\mu_{1,2,3}$-OH sites, which exert oxoanion-support interactions of intermediate strength [20,21]. These trends had already been observed for non-promoted model catalysts [21].

In order to gain insight into the cobalt speciation on the different surfaces, Grazing-Incidence X-ray absorption near edge structure (XANES) spectroscopy was carried out on the model catalysts after impregnation and two-hours 450 °C calcination. The obtained XANES spectra (Fig. 3) were compared with cobalt (II) hexa-aquo cation (cobalt nitrate) and Co_3O_4 references.

The Co K-edge XANES spectral features of model catalysts supported on the A$(11\bar{2}0)$, C(0001), M$(10\bar{1}0)$, and R$(1\bar{1}02)$ planes closely match those of the cobalt nitrate reference spectrum (Fig. 3). For instance, the maximum of the white line of the four experimental and reference Co^{2+} spectra is found at 7725 eV, while that of Co_3O_4 is found at 7730 eV. Moreover, a pre-edge peak of the model catalysts is either absent or very low in intensity, which suggests a vast majority of Co atoms being in centrosymmetric (octahedral) coordination, as opposed to Co_3O_4 and $CoAl_2O_4$ cubic spinel structure, where Co partially occupies tetrahedral (non-centrosymmetric) sites [6,37]. The former phase is associated to the formation of inactive cobalt sulfides (e.g. Co_9S_8) even at low sulfidation temperatures, the latter being lost to the alumina matrix. However, a slight shoulder at 7730 eV on the model catalysts may indicate the presence of traces of Co_3O_4.

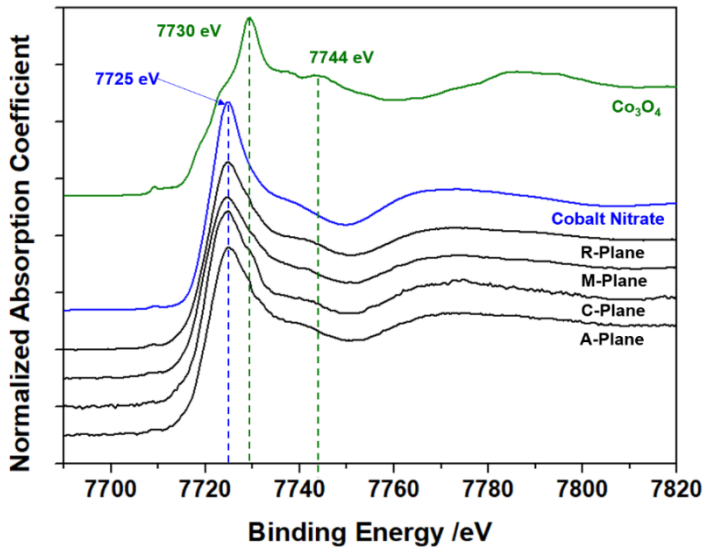

Figure 3. Co K-edge XANES spectra in perpendicular polarization (with respect to the electric field vector of the synchrotron beam) of model Co-Mo HDT catalysts supported on the A$(11\bar{2}0)$, C(0001), M$(10\bar{1}0)$, and R$(1\bar{1}02)$ crystal planes of α-Al_2O_3 in the oxide phase (after 450 °C calcination) along with cobalt nitrate and Co_3O_4 as references.

XANES spectra also do not allow us to fully exclude the presence of a minor amount of $CoMoO_4$ which should be verified by analysis of the Mo K-edge spectra [38]. Considering these results, we conclude that the large majority of Co is in octahedral coordination and well-dispersed on the model surfaces in the oxide state. Cobalt in octahedral coordination is directly associated to MoS_2 edge decoration [6].

3.2 Characterization of the model catalysts in the sulfide state

3.2.1 XPS spectral decomposition of Co2p and Mo3d regions

The model catalysts were sulfided at different temperatures ranging from 100 to 500 °C and then characterized via XPS in order to obtain a quantitative outline of Mo and Co speciation on the model catalysts, at different sulfidation temperatures. This procedure was reproduced 5-6 times per model catalyst supported on the A$(11\bar{2}0)$, C(0001), M$(10\bar{1}0)$, and R$(1\bar{1}02)$ planes. Prior to spectra analysis, the Mo and Co loadings for each model catalyst were calculated after sulfidation at 400 °C. This was carried out in order to verify the validity of Eq. 1 on catalysts subject to strong sulfiding conditions, which might lead to a surface redistribution of the metal atoms that could lead to differences in photoelectron mean free paths with respect to the oxide phase. The results displayed in Supporting Information (Table S.1) reveal no significant changes in Mo and Co loadings as well as Co/Mo ratio in the sulfide phase with respect to the oxide phase (Section 3.1). This indicates minor morphological changes upon sulfidation.

The standardized spectra processing protocol considered three possible molybdenum and cobalt species on the surface. For molybdenum, it could be present on the surface either as an oxide (MoO_3, oxidation state VI), as a mixed oxysulfide (MoO_xS_y,

oxidation state between VI and IV) or as sulfide (MoS_2, oxidation state IV). In the case of cobalt, it could be found on the substrate either as an oxide (CoO) or as a sulfide, which can in turn be a bulk phase (Co_9S_8) or cobalt decorating the edges of the MoS_2 phase (CoMoS, the active phase). All these contributions are distinguishable within their XPS region and were identified following the constraint parameters available in the Supporting Information.

An example of spectral decomposition for the Mo3d and Co2p XPS regions of a model catalyst supported on the M$(10\bar{1}0)$ plane of α-Al_2O_3 sulfided at 300 °C is displayed in Fig. 4 and results displayed in Table 3. Both molybdenum and cobalt binding energies displayed in Table 3 are in agreement with literature data [19,21,25,26].

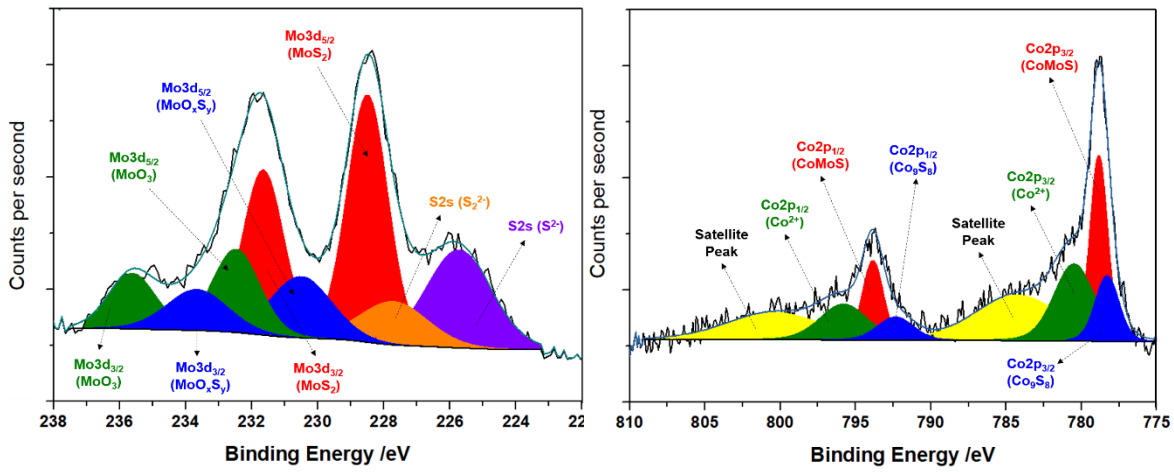

Figure 4. Spectral decomposition of the Mo3d + S2s (left) and Co2p (right) region of a model catalyst supported on the M$(10\bar{1}0)$ plane of α-Al_2O_3 after its sulfidation at 300 °C.

Gandubert et al. [25,26] identified several satellite peaks associated to each cobalt contribution. However, some of these were negligible for the model catalysts discussed in this work and the least amount of satellite peaks was used while fitting the contributions. In consequence, the satellite peaks were associated solely to the Co^{2+} contribution.

The S2p region can be used as a descriptor of the sulfidation degree as well. This region was analyzed in all the model catalysts in the sulfide state and parametrized for analysis consistency. Analysis of the S2p region of the corresponding model catalyst revealed that 65% of the surface sulfur is present as S^{2-}, directly related to the MoS_2 phase. Details about S2p decomposition is available in the Supporting Information.

Table 3. Relative proportion (%) of the different Mo and Co species on the surface of a model catalyst supported on the M$(10\bar{1}0)$ plane of α-Al_2O_3 sulfided at 300 °C obtained by XPS (see Fig. 4) with the corresponding binding energies of the $Mo3d_{5/2}$ and $Co2p_{3/2}$ peaks for each contribution.

Molybdenum		
Species	%	Binding Energy /eV
MoS_2	56.9	228.5
MoO_xS_y	20.9	230.5
MoO_3	22.2	232.5

Cobalt		
Species	%	Binding Energy /eV
Co_9S_8	16.0	778.4
CoMoS	46.6	778.9
CoO	37.4	781.4

3.2.2 Study of molybdenum speciation on the model catalysts

Figure 5 shows the evolution of the sulfidation degree (Eq. 2) throughout the studied temperature range for model catalysts supported on the A$(11\bar{2}0)$, C(0001), M$(10\bar{1}0)$, and R$(1\bar{1}02)$ crystal planes of α-Al_2O_3. C(0001) and R$(1\bar{1}02)$-plane based catalysts

display the highest and lowest sulfidation degree from 100 up to 300 °C sulfidation respectively. This is in agreement with previous results regarding model non-promoted catalysts [21]. This sulfidation trend suggests that promoted catalysts supported on the C(0001) and R$(1\bar{1}02)$ planes are associated to the weakest and strongest active phase-support interactions respectively, in line with their non-promoted counterparts [21]. However, Fig. 5 shows that the sulfidation trendline for A$(11\bar{2}0)$, M$(10\bar{1}0)$, and R$(1\bar{1}02)$ plane-based catalysts is not drastically different, contrasting with non-promoted catalysts, which displayed a clear intermediate behavior for A$(11\bar{2}0)$ and M$(10\bar{1}0)$-based ones [21]. Therefore, cobalt incorporation appears to level out the differences among A$(11\bar{2}0)$, M$(10\bar{1}0)$, and R$(1\bar{1}02)$ planes.

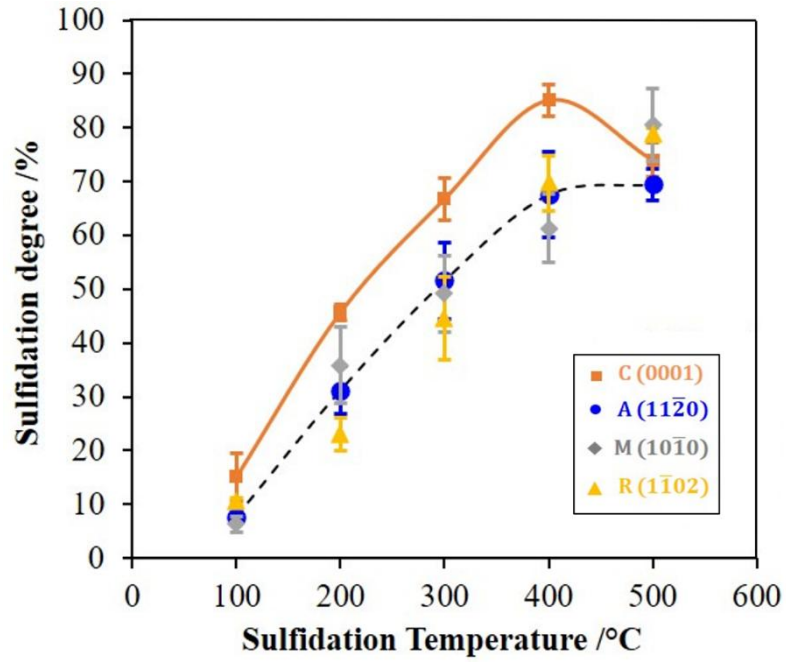

Figure 5. Sulfidation degree for model Co-promoted Mo-based HDT catalysts supported on the C(0001), A$(11\bar{2}0)$, M$(10\bar{1}0)$, and R$(1\bar{1}02)$ crystal planes of α-Al_2O_3 as a function of the sulfidation temperature. Error bars correspond to the average standard deviation. The orange trendline corresponds to the one exhibited by the C(0001) plane whereas the dotted trendline follows the A$(11\bar{2}0)$ plane.

3.2.3 Microscopy study of the model surfaces in the sulfide state

AFM imaging of model catalysts in the sulfide state allowed to evaluate post-sulfidation dispersion at a temperature displaying the biggest differences in Mo speciation (300 °C, Fig. 6). The topographic profile of C(0001) plane-based catalysts shows a poorly dispersed active phase in comparison with the rest of the model catalysts, with aggregates 6-12 nm tall and 3-21 nm long in average. Indeed, the dispersion profile of C(0001) plane-based sulfided catalysts maintains a similarity with its analogue in the oxide phase, suggesting that the weak strength of metal-support interactions is maintained upon sulfidation. Nevertheless, AFM imaging of C(0001) plane-based catalysts also revealed a decrease in the average particle diameter of around 40 nm with respect to the oxide phase. In addition, the C(0001) plane topographic profile shows slightly taller aggregates on average for promoted samples (this work) than for non-promoted ones [21], the latter ranging from 2-8 nm tall. This slight increase in height may be attributable to cobalt promotion, which has been proposed to decrease the strength of metal-support interactions by stabilizing the edges of MoS_2 [10]. However, AFM profiles show little to no change in particle width upon cobalt promotion with respect to their non-promoted counterparts, indicating that cobalt promotion induces an increase in stacking, but not in lateral growth. Indeed, some studies [39,40] have discussed the key role of cobalt in the inhibition of particle growth, in agreement with our AFM results.

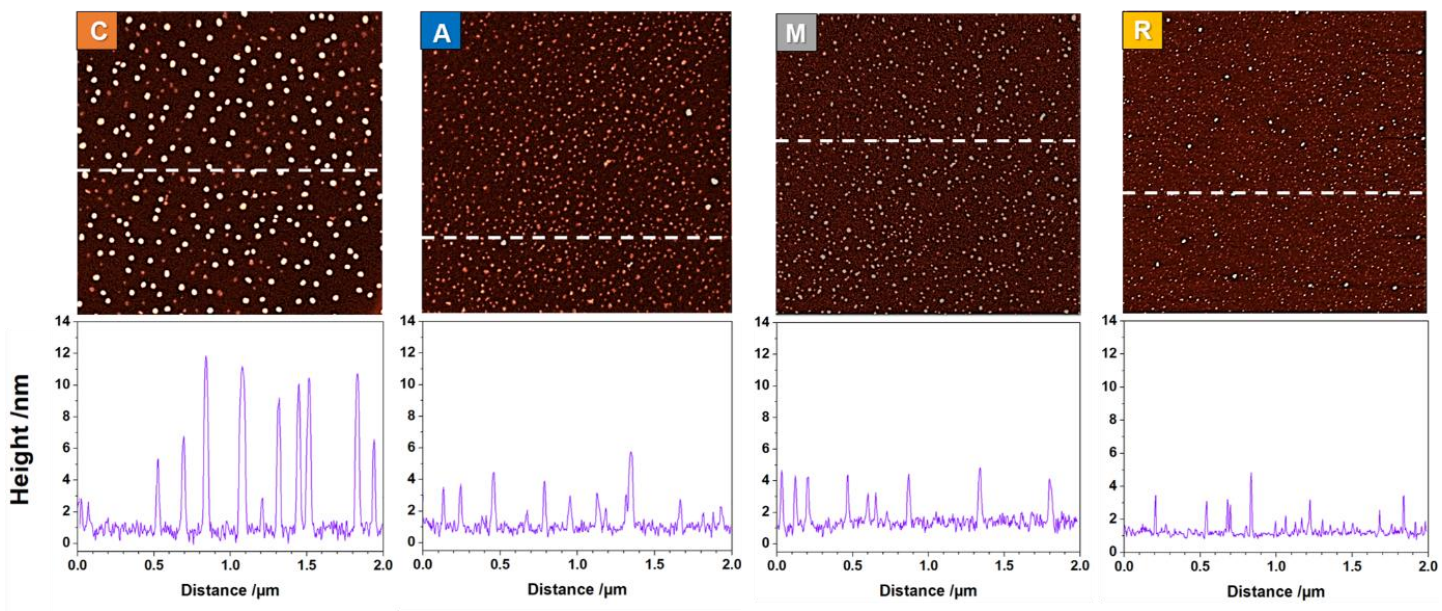

Figure 6. 2 µm x 2 µm AFM images (top) and height profiles (bottom) for a series of Co-Mo-based model catalysts supported on the C(0001), A$(11\bar{2}0)$, M$(10\bar{1}0)$, and R$(1\bar{1}02)$ crystal planes of α-Al_2O_3 after sulfidation under H_2S/H_2 at 300 °C. The white dashed line represents the segment of the image from which the height profile was obtained.

Figure 6 also reveals the more dispersed nature of A$(11\bar{2}0)$, M$(10\bar{1}0)$, and R$(1\bar{1}02)$ plane-based catalysts in the sulfide state, compared to the C(0001)-plane ones. Similarly to C(0001) plane-based catalysts, Co-promoted MoS_2 supported on the A$(11\bar{2}0)$, M$(10\bar{1}0)$, and R$(1\bar{1}02)$ planes show higher particle height (1.0 to 4.0 nm) than their non-promoted counterparts (1.0 to 1.5 nm) [21]. A 4 nm aggregate height would correspond to a stacking number between 5 and 6 considering 3.08 and 3.49 Å slab height and interlayer distance respectively [41].

A more refined evaluation of metal dispersion was obtained by TEM imaging (Fig. 7) of the model catalysts sulfided at 400 °C. The sulfidation temperature for TEM analysis was chosen to be the same as the reaction temperature (see Section 2.4). Statistical analysis of CoMoS slab lengths and stacking number for each model catalyst is given in Fig. 8. The slabs (visible in black, Fig. 7) appear in higher density in regions with a darker background, which indicate a higher alumina concentration.

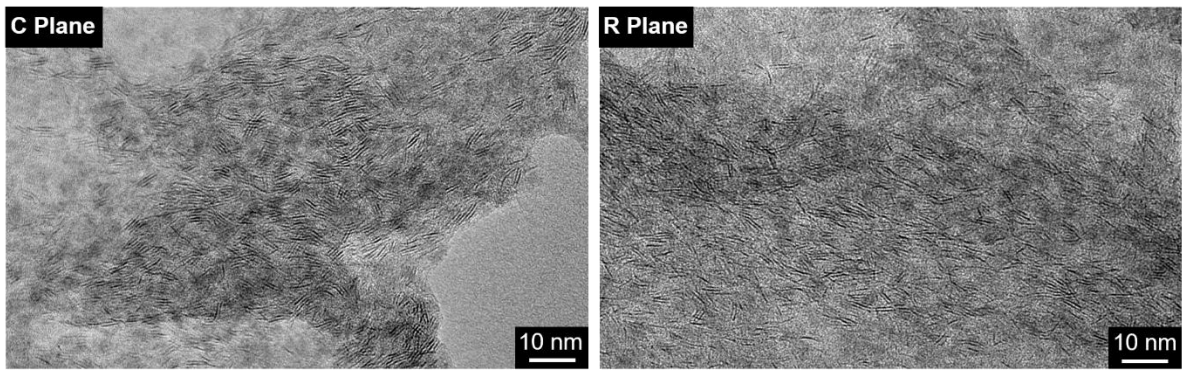

Figure 7. Representative TEM images of model CoMo HDT catalysts supported on the C(0001) and R$(1\bar{1}02)$ crystal planes of α-Al_2O_3 sulfided at 400 °C.

Figure 7 shows a higher concentration of stacked CoMoS slabs on the C(0001) plane, compared to the more dispersed nature of the active phase on the R$(1\bar{1}02)$ plane catalysts. This goes in agreement with the AFM topographic profile from both crystal planes in the sulfide state (Fig. 6).

Statistical analysis of TEM images of the four crystal planes (at least 200 slabs per plane) revealed slab lengths typical of promoted MoS_2/Al_2O_3 catalysts [4]. The longest slabs in average lie on the C(0001) plane, whereas the shortest are supported on the R$(1\bar{1}02)$ plane with length of 4.5 ± 0.1 and 3.5 ± 0.1 nm long respectively, on average. An intermediate average length is exhibited by the A$(11\bar{2}0)$ and M$(10\bar{1}0)$ plane-based catalysts with slabs of 3.9 ± 0.1 and 3.8 ± 0.1 nm long respectively. Comparison of the slab lengths of Co-promoted model catalysts (this work) to non-promoted ones (Bara et al. [21]) revealed a decrease in average slab length of 0.6 to 0.2 nm. This decrease in slab length has been previously reported upon cobalt promotion [42,43], with a 0.6 nm decrease in slab length on traditional porous catalysts; it can be attributed to the stabilizing effect of Co on the edge energy.

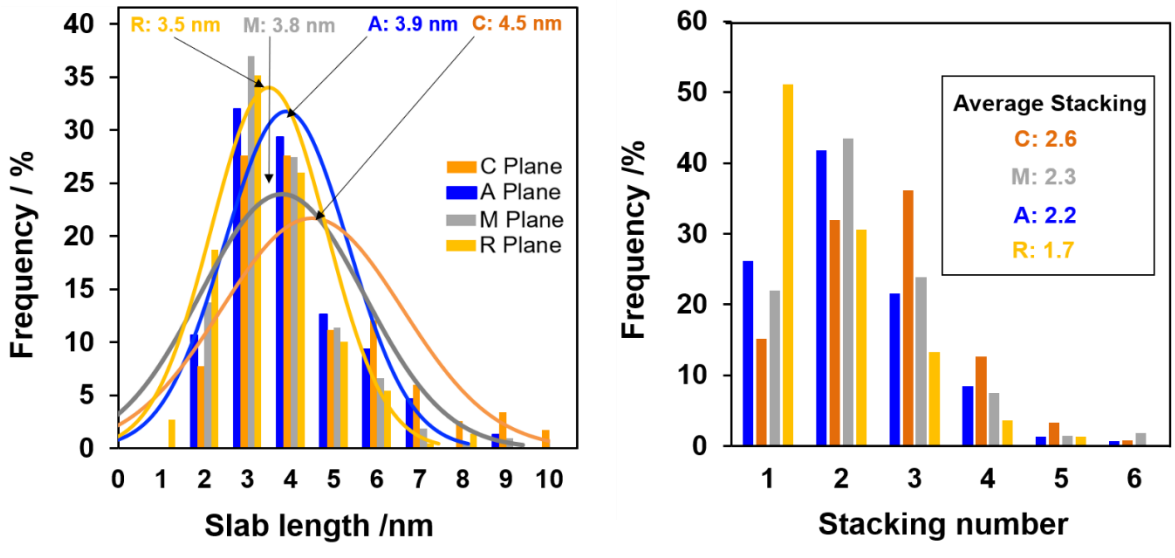

Figure 8. Slab length (left) and stacking number (right) distribution for model Co-promoted Mo-based HDT catalysts supported on the C(0001), A$(11\bar{2}0)$, M$(10\bar{1}0)$, and R$(1\bar{1}02)$ crystal planes of α-Al_2O_3 sulfided at 400 °C obtained via TEM image analysis.

The average stacking number is another parameter used to describe the dispersion of the supported active phase. TEM image analysis allows one to distinguish stacks of individual CoMoS slabs on the alumina surface, as seen in Fig. 7. Statistical analysis of TEM images from the different model catalysts revealed a surface-dependent stacking number of CoMoS slabs (Fig. 8, right). C(0001) plane-based catalysts display the highest stacking number with 2.6 slabs per aggregate on average, with 53% of them belonging to an aggregate of two or more slabs. The lowest stacking number is exhibited by the R$(1\bar{1}02)$ with 1.7 in average, with 82% of particles belonging to a single or double slab unit. A$(11\bar{2}0)$ and M$(10\bar{1}0)$-based catalysts showed both 2.2 and 2.3 slabs on average per particle, with 68% and 65% of them belonging to a two or one-slab particle, respectively.

Finally, we observe that the average stacking number of all model catalysts obtained by AFM is consistently higher than those obtained by TEM measurement. We suggest that the difference between both methods can be explained by the ability of AFM to probe aggregates. These could be formed by accretion of few particles with lower stacking number, such as the ones probed by TEM.

3.2.4 Cobalt speciation on the model catalysts

The speciation of cobalt on the different crystal planes was analysed by XPS at different sulfidation temperatures. The promotion extent (Eq. (3), Fig. 9) was calculated from the Co2p peak intensities. The model catalysts show an increasing promotion extent with sulfidation temperature up to 400 °C. After this maximum, the promotion extent decreases, showing a bell-shape pattern already described in the literature with traditional supports [25].

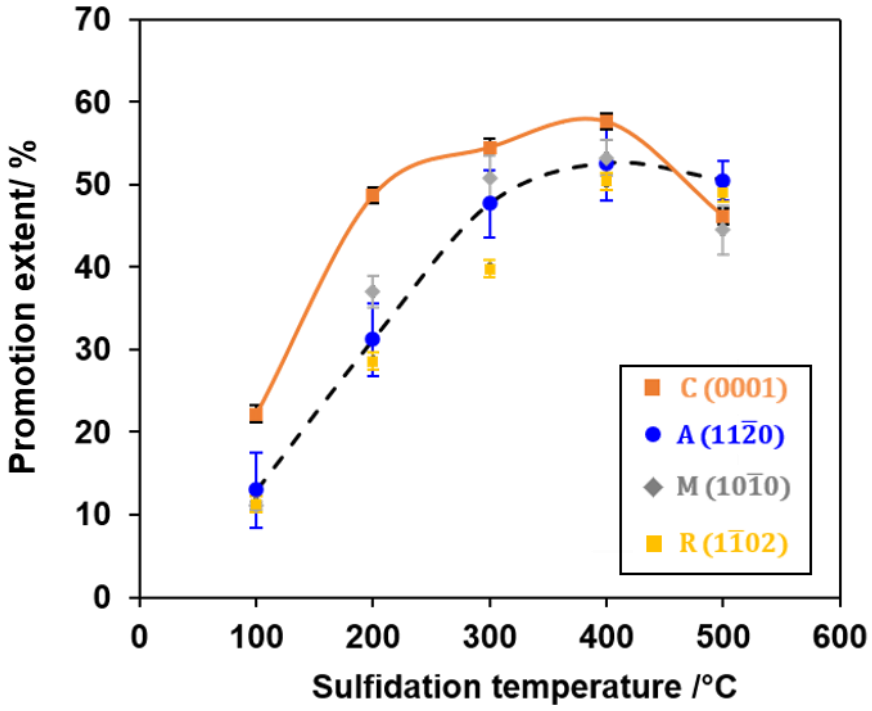

Figure 9. Promotion extent for model Co-promoted Mo-based HDT catalysts supported on the C(0001), A$(11\bar{2}0)$, M$(10\bar{1}0)$, and R$(1\bar{1}02)$ crystal planes of α-Al_2O_3 as a function of the sulfidation temperature. Error bars correspond to the average standard deviation. The orange trendline corresponds to the one exhibited by the C(0001) plane whereas the dotted trendline follows the A$(11\bar{2}0)$ plane.

Indeed, Gandubert et al. [25] found that cobalt incorporated into the CoMoS phase peaked at around 350 °C (for a Co/Mo ratio of 0.5), with around 50% of the atoms being part of the mixed CoMoS structure. In the case of our model catalysts, this maximum is found at 400 °C with up to 62.5% of cobalt atoms incorporated into the mixed phase (case of the C(0001) plane). Similarly to the trendline observed by Gandubert et al. [25], the model catalysts presented in this work unanimously show a decrease in the promotion extent at 500 °C sulfidation, which probably extends to higher sulfidation temperatures. This decrease has been attributed to an increase in the concentration of the Co_9S_8 phase, which forms at the expense of the CoMoS phase. As a matter of fact, XPS shows that up to 22% of Co_9S_8 can be detected at 500°C on the model catalysts vs. about 15% from 200 to 400 °C (see supporting information). Hence, a de-promotion of the active phase occurs at sulfidation temperatures higher than 400 °C for all model catalysts regardless of the nature of their support.

In order to clarify the origin of the surface-dependence in cobalt promotion of MoS_2, the promotion extent was plotted as a function of the sulfidation degree for all surfaces (Fig. 10)

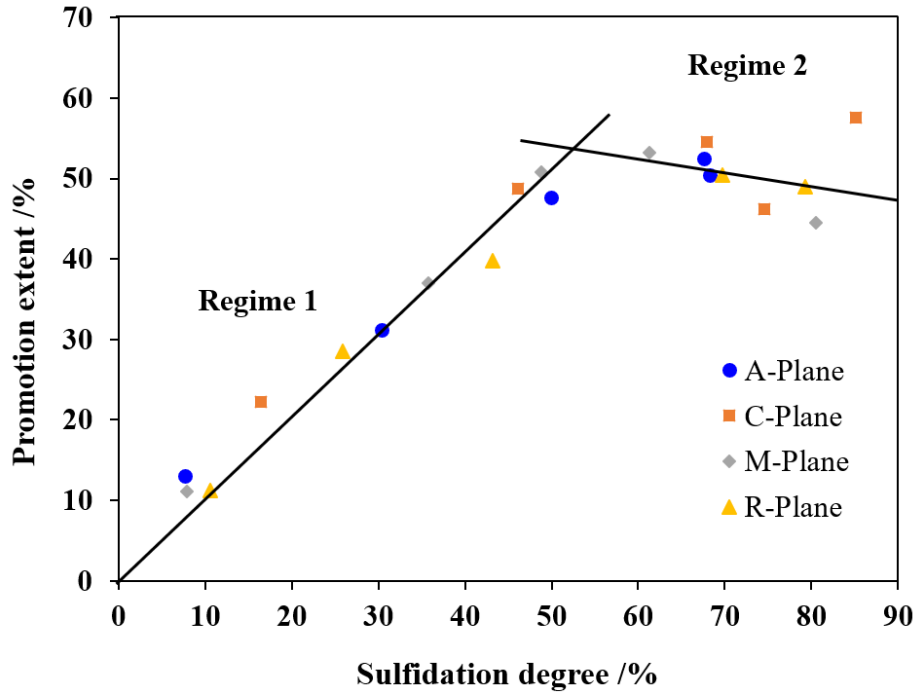

Figure 10. Promotion extent (%) of model CoMo catalysts supported on the C(0001), A$(11\bar{2}0)$, M$(10\bar{1}0)$, and R$(1\bar{1}02)$ crystal planes of α-Al_2O_3 as a function of the sulfidation degree (%).

Figure 10 reveals the existence of two regimes. In Regime 1, we see a clear linear dependency, suggesting that cobalt edge decoration is conditioned by the emergence of the MoS_2 phase. Moreover, the trend associated to Regime 1 reveals that regardless of the crystal plane, cobalt edge decoration occurs almost simultaneously to the formation of MoS_2. In Regime 2, we see a slightly decreasing promotion extent with increasing sulfidation degree. This implies that cobalt promotion of MoS_2 is less favorable above 400 °C with respect to the formation of bulk cobalt sulfides (Co_9S_8) since the latter are thermodynamically more stable.

We infer from the obtained results that the formation of the promoted active phase is contingent on the formation of MoS_2, which is clearly surface-dependent as shown in Fig. 5. Hence, the promotion extent shown in Fig. 9 logically parallels the sulfidation degree with a maximum promotion extent for the C(0001) plane up to 400 °C. Similarly, results for the Co-promotion on the M$(10\bar{1}0)$, A$(11\bar{2}0)$, and R$(1\bar{1}02)$ planes are very similar in line with a common trend line for the sulfidation degree on these three surfaces.

3.2.5 Qualitative evaluation of cobalt speciation by GI-XAS

Grazing-incidence X-ray absorption spectroscopy (XAS) was used as a complementary technique to evaluate the extent of sulfidation on the model catalysts (Fig. 11) by comparison with references in the oxide (cobalt nitrate or Co^{2+}) and sulfide states (Co_9S_8). It has to be noted that XANES alone cannot discriminate Co_9S_8 from the CoMoS phase although a chemometric analysis method has been recently developed to extract the CoMoS contribution from EXAFS spectra of CoMo catalysts [33].

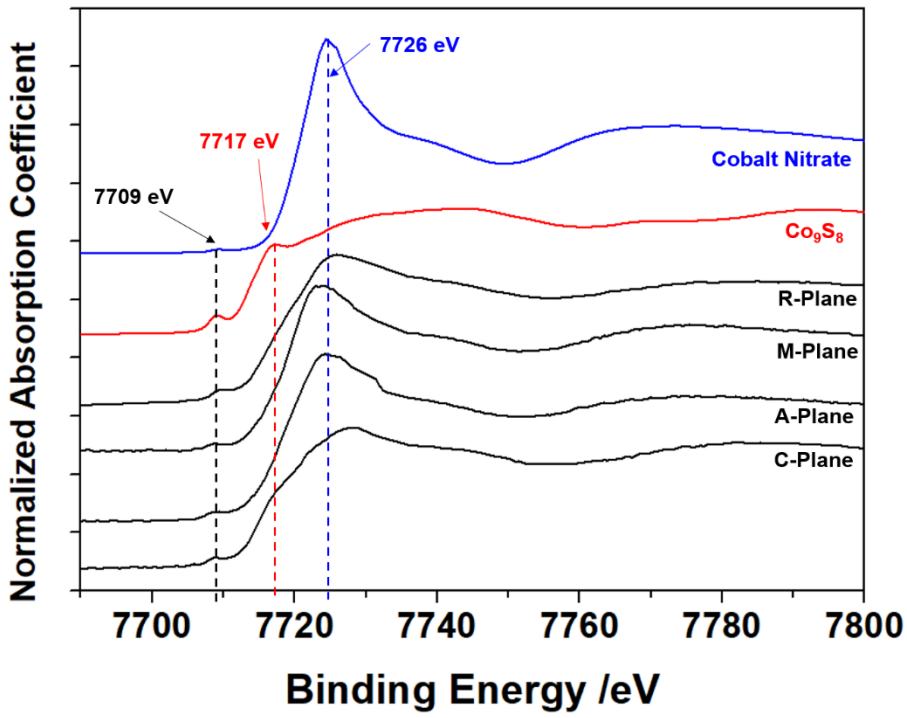

Figure 11. XANES spectra of model Co-Mo HDT catalysts supported on the C(0001), A$(11\bar{2}0)$, M$(10\bar{1}0)$, and R$(1\bar{1}02)$ crystal planes of α-Al_2O_3 (black spectra) in parallel polarization after sulfidation at 300 °C. XANES spectra of reference cobalt nitrate (blue) and Co_9S_8 (red) are also shown.

From the Co^{2+} and Co_9S_8 reference spectra (Fig. 11), we observe three different features that can serve as indicators for the sulfidation degree: the intense white line of Co^{2+} at 7726 eV, the white line of Co_9S_8 at around 7717 eV and the intense pre-edge of Co_9S_8 at 7709 eV. As seen in Fig. 11, the white line corresponding to cobalt (II) oxide is visibly aligned with the ones displayed by the A$(11\bar{2}0)$, M$(10\bar{1}0)$, and R$(1\bar{1}02)$ planes, while that of C(0001) plane catalyst displays a less oxidic-like contour. Indeed, the XANES spectrum of this latter surface resembles much more that of Co_9S_8, suggesting a more sulfidic nature for cobalt on this surface in full agreement with XPS results (Fig. 9).

The EXAFS spectra of the C(0001) plane-based catalyst were studied for both parallel and perpendicular polarizations. Fig. 12 (left) shows that the forward Fourier transforms from both polarizations are virtually identical, indicating no orientation effect for cobalt species. It must be noted that Co K-edge XAS is probably less sensitive than Mo K-edge to a possible orientation-dependence of the CoMoS slabs since Co is mostly isolated and only decorating the edges of the slabs. The first-neighbor peak of the EXAFS spectra from both polarizations are in between those of sulfided and oxidic cobalt references with a first neighbor at a radial distance between the short Co-O bond (around 2.07 Å), and the longer Co-S distances (2.13, 2.21, and 2.39 Å) reported in the literature [33].

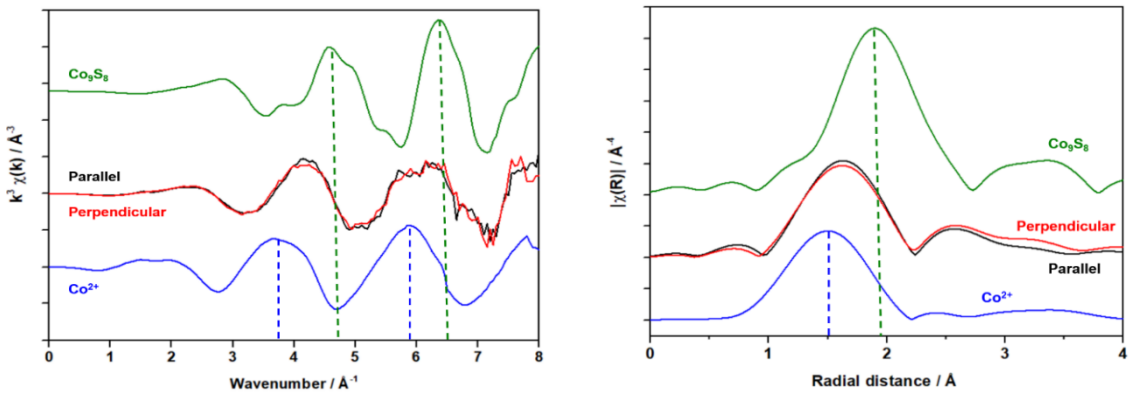

Figure 12. **Left**: k^3-weighted Co K-edge EXAFS spectra of a model Co-Mo catalyst supported on the C(0001) plane of α-Al_2O_3 in parallel (black) and perpendicular (red) polarizations along with that of Co_9S_8 and Co^{2+} reference spectra. **Right**: Fourier Transforms (uncorrected for phase shift) of the corresponding EXAFS spectra with Δk = 3-8 $Å^{-1}$.

3.3 Cobalt substitution degree of model catalysts

The substitution of Mo atoms by Co at the M and S edges of the MoS_2 structure can be described through the substitution degree, i.e. the proportion of Mo atoms substituted by Co. The calculation (see Section 2.3.4) takes into consideration the promotion and sulfidation degrees, as well as the number of Mo atoms in edges and corners (from the slab length) for a slab with a perfectly hexagonal geometry, as seen in Fig. 13 (left).

The calculated substitution degree (Table 4) reveals 94% Co substitution for A$(11\bar{2}0)$ plane-based catalysts, around 90% for C(0001) and M$(10\bar{1}0)$-based and 80% for R$(1\bar{1}02)$ plane-based. These results are not in agreement with a complete substitution of the S-edge and a partial substitution of the M-edge (≈50 %) at typical HDS conditions as proposed before [11,44] which would yield a substitution degree of ≈75 % if we consider a regular hexagon. However, there are both theoretical and experimental evidences that the geometry of the CoMoS slab is not perfectly hexagonal at HDS conditions [45] and our results suggest either full S and M edge substitution (especially for C(0001), A$(11\bar{2}0)$, and M$(10\bar{1}0)$ plane-based catalysts) or higher S/M ratios with respect to conventional catalysts.

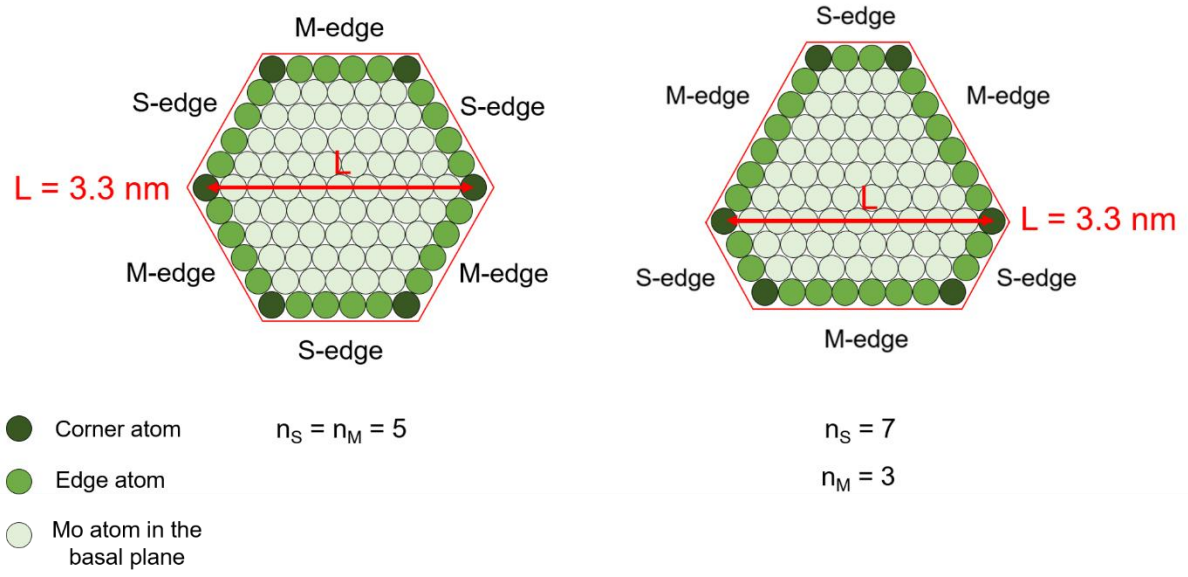

Figure 13. Simplified schematic representation of a CoMoS slab of 3.3 nm long with perfectly hexagonal geometry (left) and distorted hexagonal geometry with two different sides (right). For the latter, the M-edge is enhanced by a ratio 7:3 with respect to the S-edge. n_S and n_M are the number or Co or Mo atoms belonging to the S and M edges, respectively.

Table 4. Average length, mean atomic ratio in the slabs and substitution degrees for the model Co-promoted Mo-based catalysts supported on the C(0001), A$(11\bar{2}0)$, M$(10\bar{1}0)$, and R$(1\bar{1}02)$ crystal planes of α-Al_2O_3 after 400 °C sulfidation

Model catalyst	C-Plane	A-Plane	M-Plane	R-Plane
Length **/nm**	4.5	3.9	3.8	3.5
$\left(\frac{Co}{Mo}\right)_{slab}$	0.29	0.36	0.35	0.36
Substitution degree **/%**	90	94	91	80

3.4 Catalytic activity of model systems in thiophene hydrodesulfurization

Thiophene hydrodesulfurization was carried out using four identical samples prepared on the same crystal plane for a total of 4 cm^2 surface area. The Mo and Co loadings (4 and 2 at·nm^{-2}) of the model catalysts would correspond to ~16 wt% MoO_3 and ~5 wt% CoO for a traditional 200 $m^2 \cdot g^{-1}$ γ-Al_2O_3 powder support in agreement with industrially-relevant systems [46]. A 1 cm^2 single crystal catalyst (~200 mg) with these loadings contains roughly 0.6 and 0.3 nmol of Mo and Co on its surface respectively. However, the same weight of a γ-Al_2O_3 powder catalyst (200 $m^2 \cdot g^{-1}$) will contain 400 000 times more Mo and Co (around 260 and 133 µmol respectively). This difference of several orders of magnitude in metal loading shows the difficulty in obtaining measurable catalytic activity with model catalysts. This conundrum was already faced by Kishan et al. [47,48] who obtained yields of around 0.6% for additive-free CoW/SiO_2 thin films of 5 cm^2. Nonetheless, even with such very low yields, Kishan et al. [47] managed to observe

meaningful differences in catalytic activity among the tested model catalysts using batch configuration. Following this precedent, our model reaction was carried out under batch configuration over 24 h and reproducible conversions between 0.1 and 0.4 % could be determined. The overall conversions of the model catalysts are displayed in Fig. 14 along with the standard deviation obtained from repeated measurements (five for M$(10\bar{1}0)$-based catalysts and two for A$(11\bar{2}0)$, C(0001), and R$(1\bar{1}02)$-based catalysts).

Figure 14 shows that A$(11\bar{2}0)$ plane-based catalysts exhibit higher catalytic activity than the rest, with an average conversion of 0.38%. M$(10\bar{1}0)$ plane-based catalysts resulted in the second-most active ones with 0.21% conversion. At last, R$(1\bar{1}02)$ and C(0001) plane-based catalysts show conversions of 0.16% and 0.13% on average. The normalized activities followed the same trend.

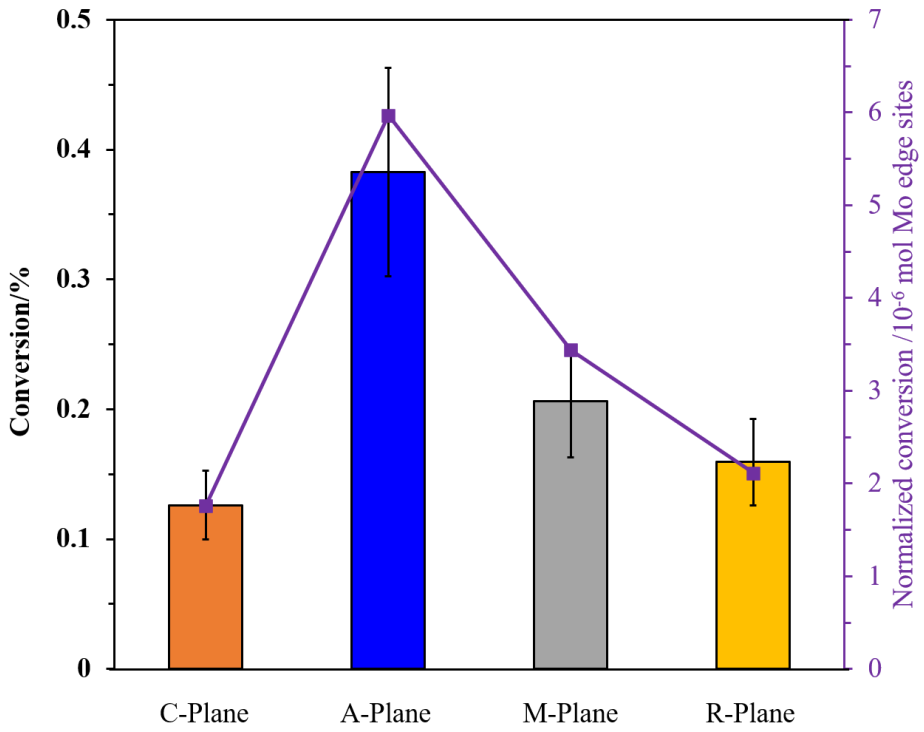

Figure 14. Histograms displaying raw thiophene conversion (Eq. 6) towards hydrodesulfurization products for model Co-promoted Mo-based HDS catalysts supported on the C(0001), A$(11\bar{2}0)$, M$(10\bar{1}0)$, and R$(1\bar{1}02)$ crystal planes of α-Al_2O_3 sulfided at 400 °C for a thiophene hydrodesulfurization reaction conducted at 400 °C during 24 h in a batch mode (left Y-axis). Error bars correspond to the standard deviation over two to five measurements. In violet (right Y-axis): normalized conversion values (conversion per mole of Mo occupying corner or edge sites, Eq. 7).

Figure 15 displays the relative selectivity (in %) for the five hydrodesulfurization products for each model catalyst. 1-butene is the main HDS product for all model catalysts regardless of the support, ranging from 33 to 44% of the total products. This result is in agreement not only with the results reported by Kishan et al. [47], but also with studies based on traditional supports under typical HDS conditions [49,50]. The second most important HDS product is consistently 1,3-butadiene, with a relative selectivity ranging from 19 to 25% depending on the substrate. On third and fourth positions, both trans and cis isomers of 2-butene are found, respectively. Trans-2-butene accounts for 18-20% of all HDS products while the cis isomer ranges from 8-14%. This higher selectivity towards the trans isomer was also consistently reported by Kishan et al. [47] and studies involving traditional catalysts [49,50]. Finally, n-butane appears as the lowest concentration product, making up from 3 to 7% of thiophene HDS products. The formation of n-butane requires an additional hydrogenation step for 1-butene and 2-butene isomers, which renders its formation limited with respect to the rest of the HDS products.

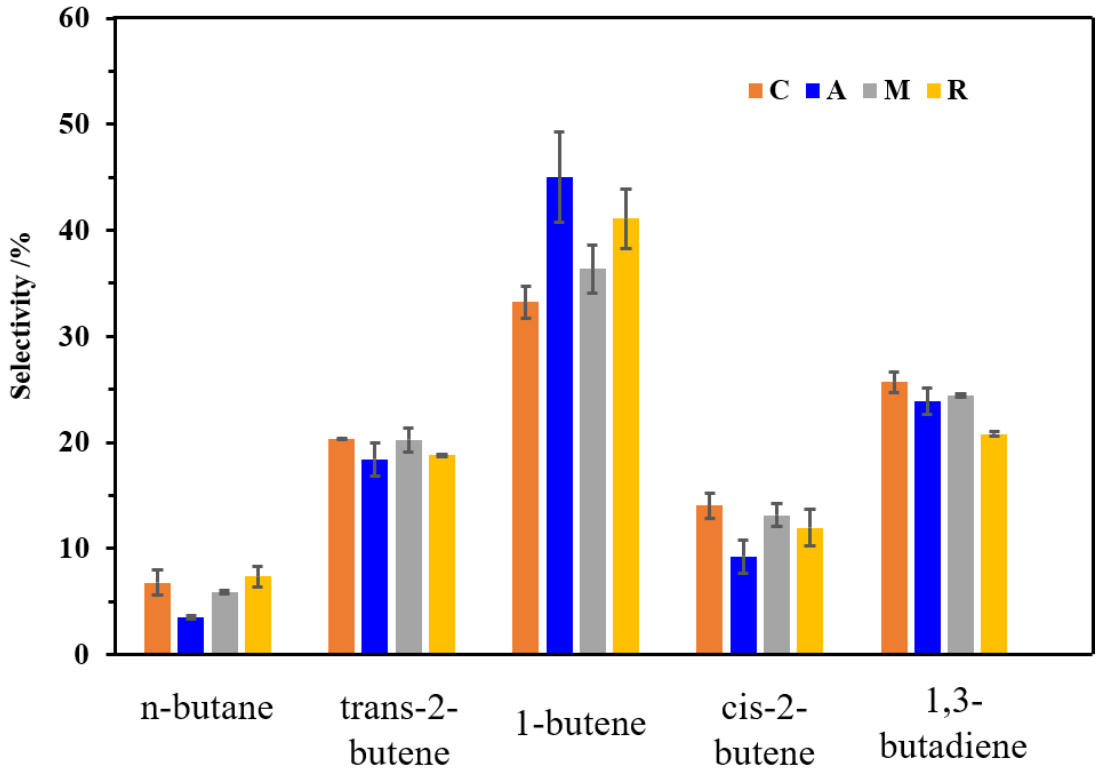

Figure 15 Selectivity in thiophene hydrodesulfurization for model Co-promoted Mo-based HDS catalysts supported on the C(0001), A$(11\bar{2}0)$, M$(10\bar{1}0)$, and R$(1\bar{1}02)$ crystal planes of α-Al_2O_3 sulfided at 400 °C. Reaction conducted at 400 °C during 24 h in batch mode. Order of products corresponds to their chronological appearance on the chromatogram.

The unusually high concentration of 1,3-butadiene in our results is worth highlighting since all thiophene HDS selectivity studies report either a consistently low yield for this hydrocarbon or no concentration at all [47,51–53] while our results show that it is the most important HDS product after 1-butene. We infer that the significant contribution of 1,3-butadiene is due to the extremely low overall conversion, as this species is an intermediate in the DDS pathway.

4. Discussion

4.1 Relationship between Mo-support interactions and the genesis of the active phase.

The role of the alumina support is demonstrated in this work and is probably the most apparent in the evolution of the sulfidation degree with temperature (Fig. 5). These results indicate that regardless of the crystal plane orientation, no complete sulfidation was attainable, even above 400 °C. On the contrary, complete sulfidation of most unsupported (bulk) transition metal oxides is typically achieved as early as 300 °C [54]. The role of the oxide support (e.g. alumina) on sulfidation of dispersed transition metal oxides has already been demonstrated in past works and uncomplete sulfidation of supported MoOx has been usually assigned to the presence of Al-O-Mo bonds that anchor MoS_2 to the support [55–59] In that sense, at least a fraction of supported Mo atoms will not be part of a pure MoS_2 matrix, but will be rather associated to species with oxidation state between that of MoS_2 and MoO_3.

The effect of the alumina surface orientation on the sulfidation degree can be noted on Fig. 5 with the C(0001) plane-based catalysts displaying the highest sulfidation degree from 100 °C up to 400 °C sulfidation. This behavior is attributed to weak active phase-support interactions associated to Al_{6C}-μ_2-OH sites, constituting the hydrated surface of the C(0001) plane.[19,36] These weak interactions lead to poor oxoanion dispersion (AFM, Fig. 2), maintained in the sulfide state as well (AFM, Fig. 6). TEM results also show that C(0001) plane-based catalysts exhibit both a larger average slab length compared to the rest (37% of slabs longer than 5 nm) and the highest stacking number as well. In conclusion, key features of the active phase (high sulfidation and low dispersion) may be assigned to weak active phase-support interactions for C(0001) plane-based catalysts.

On the other hand, R$(1\bar{1}02)$-plane based catalysts exhibit the lowest sulfidation degree at low sulfidation temperatures (200 and 300°C), which can be explained by the nature of R$(1\bar{1}02)$ plane sorption sites as well, which have been identified as surface Al_{4C}-μ_1-OH sites [24] and associated to strong metal-support interactions.[21] In addition, these strongly-interacting sites account also for the highly-dispersed nature of the CoMoS phase as evidenced by AFM and TEM imaging.

The sulfidation degree and Co-promotion of A$(11\bar{2}0)$ and M$(10\bar{1}0)$-based catalysts are similar to those for the R$(1\bar{1}02)$-plane. However, the dispersion is somewhat different on the former orientations. Indeed, A$(11\bar{2}0)$ and M$(10\bar{1}0)$ planes display slightly larger slabs (3.8-3.9 nm) and higher average stacking numbers (2.2-2.3) with respect to R$(1\bar{1}02)$ plane-based ones (length

=3.5 nm and average stacking number = 1.7). These results suggest that A$(11\bar{2}0)$ and M$(10\bar{1}0)$ plane-based catalysts are subject to weaker active phase-support interactions than R$(1\bar{1}02)$-based ones.

The previous conclusions are in line with those obtained on non-promoted systems with increasing metal-support interactions in the following order : C(0001) < A$(11\bar{2}0)$ and M$(10\bar{1}0)$ < R$(1\bar{1}02)$ [21]. However, statistical analysis of the stacking number of CoMoS slabs supported on the four crystal planes (Fig. 8, right) reveals a significant increase in the overall average stacking number of Co-promoted systems compared to non-promoted ones supported on the same substrates. Bara et al. [21] reported from 60% to 80% single MoS_2 slabs on α-Al_2O_3 substrates, depending on the crystal plane, in contrast to the 15% to 51% range observed for CoMoS slabs. The overall increase in stacking number upon cobalt promotion suggests a weakening effect exerted by Co on the active phase-support interactions. Incorporation of cobalt would lead to the weakening the Mo-O-Al bonds of small MoS_2 particles and allow the stacking of MoS_2 layers instead of lateral growth, as suggested by our AFM results (Fig. 6). The same pattern of slab length reduction and increased stacking was reported by Berhault et al. [42], who reported an increase of almost four slabs per aggregate upon cobalt promotion of MoS_2 supported on traditional alumina with respect to non-promoted samples.

4.2 Relationship between the nature of the support and the catalytic activity

The surface-dependent genesis of the CoMoS phase extends to the catalytic activity as well, since Fig. 14 shows that model catalysts exhibit different thiophene hydrodesulfurization conversions depending on the nature of the surface orientation. The A$(11\bar{2}0)$ plane-based catalysts are notably more active than the other model catalysts. In order to exclude a difference in the number of active sites, a normalized conversion was calculated (Fig. 14) by dividing the conversion by the number of reaction sites, i.e. moles of corner and edge Mo sites (see Section 2.4). The same trend as that for the raw conversion is obtained which demonstrates that the changes in conversion can be related to differences in intrinsic activity of reaction sites. In order to rationalize these results, we may consider different descriptors of the promoted active phase that could help rationalize the catalytic behavior of the model catalysts (Table 5).

Table 5. Comparative summary of different descriptors of the CoMoS phase on model hydrotreating catalysts supported on the A$(11\bar{2}0)$, C(0001), M$(10\bar{1}0)$, and R$(1\bar{1}02)$ crystal planes of α-Al_2O_3 at 400 °C (HDS reaction and sulfidation)

Descriptor	C(0001)	A$(11\bar{2}0)$	M$(10\bar{1}0)$	R$(1\bar{1}02)$
Catalytic activity*	Lowest	Highest	Intermediate	Intermediate
Co promotion extent	Highest	Lowest	Lowest	Lowest
Co substitution extent	Highest	Highest	Highest	Lowest
Stacking number (TEM)	Highest	Intermediate	Intermediate	Lowest

*The catalytic activity refers to the normalized conversion, which takes into consideration the sulfidation degree and the slab length parameters.

From Table 5, it appears that none of the descriptors can explain by themselves the high activity of A$(11\bar{2}0)$-based catalysts since none of them point toward a peculiar behavior of this surface orientation. However, it was shown that morphological parameters (stacking number and slab length) for A$(11\bar{2}0)$ and M$(10\bar{1}0)$-based catalysts display relatively intermediate behaviors as compared to R$(1\bar{1}02)$ and C(0001)-based catalysts which was assigned to intermediate active-phase support interactions. Hence, it can be suggested that the high catalytic activity of A$(11\bar{2}0)$-based and (to a much lesser extent) M$(10\bar{1}0)$-based catalysts may arise from a compromise between strong and weak active phase-support interactions.

Other precedents in the literature have invoked a support effect to explain the trends in catalytic activity. For instance, Berhault et al. [42] revealed that alumina and silica-supported CoMo catalysts holding similar stacking numbers (95% and 88% of single slabs respectively) exhibited a major activity difference, with 13% higher TOF on alumina-supported catalysts, suggesting an intrinsic effect of the support on the activity. Laurenti et al.[60] used three alumina polymorphs and found that δ-Al_2O_3-supported catalysts exhibited higher activity than two different γ-Al_2O_3 polymorphs by factors of 2.5 and 1.7. Moreover, the stacking number

and metal sulfidation degree was the same for δ and tetragonal γ-Al_2O_3, suggesting an intrinsic effect of the support on the overall activity, possibly attributed to support-induced electronic effects.

In the present work, the role of the support is suggested to arise from metal-support interactions of intermediate strength resulting in higher HDS activity. Two hypotheses may help explain the relationship between the nature of active phase-support interactions and catalytic activity.

The first one is the role of the metal-support interactions on the CoMoS slabs morphology. In a recent contribution, Dominguez-Garcia et al. [61] found that the morphology of MoS_2 slabs on non-promoted Mo-based catalysts was largely affected by the nature of the oxide support (SiO_2, Al_2O_3, TiO_2). The S-/M- edge ratio is increasing with decreasing strength of metal/support interactions (SiO_2 < Al_2O_3 < TiO_2). Indeed, the slab morphology is controlled by the surface free energy which, in turn, can be determined by the strength of active phase-support interactions [62]. In addition, it was reported by Dominguez-Garcia et al. [61] that higher S/M edge ratios generally resulted in higher turnover frequencies in thiophene HDS (except for TiO_2-supported catalysts). However, the conclusions reached by Dominguez-Garcia et al. [61] cannot explain the optimum in catalytic activity observed for our model systems for intermediate metal/support interactions. Indeed, highest S-/M- edge ratios would be attained through weakest metal/support interactions (e.g. C(0001)-based catalysts), which should then lead to the highest activity for the latter surface while it shows the poorest performance.

Second, metal-support interactions may impact metal-sulfur (M-S) bond energy in CoMoS slabs. Indeed, M-S energy is a fundamental parameter in hydrodesulfurization reaction, influencing the adsorption, surface reaction and desorption of reactants and products. Toulhoat and Raybaud [63,64] computed the bulk M-S energies of different transition metal sulfides which were plotted versus experimental HDS activity, resulting in a volcano-shaped curve, with CoMoS catalysts close to the peak of such curve (i.e., the intermediate bulk M-S energy of CoMoS with respect to other active phases results in a higher activity). While M-S bond energies were determined from bulk, unsupported sulfide slabs, it may also be hypothesized that M-S bond energies can be largely affected by metal-support interactions. Such effect has been suggested for TiO_2 supported MoS_2 where sulfur-deficient clusters are favored over alumina-supported catalysts due to stronger interactions with TiO_2 [55]. Hence, stronger metal-support interactions would lower M-S bond energy in line with a reasoning on bond order preservation of surface anchored MoS_2 slabs. In other words, optimal M-S bond strengths for HDS would be attained through metal-support interactions of intermediate strength, while stronger and weaker interactions would result in lower activities. Hence, results of Fig. 14 may be an alternative version of a volcano-shaped curve (following the Sabatier principle) by considering metal-support interactions as a key descriptor of the catalytic activity through a direct influence on M-S bond energy. However, the role of Co has also to be taken into account since it was also shown that Co weakens the interactions between the CoMoS slabs and the support [65] which should in turn impact M-S bond energy. Hence optimal M-S bond energy (maximum of the volcano plot) may result from a trade-off between metal-support interactions and Co promotion.

Further research should be undertaken in order to confirm this latter hypothesis through DFT calculations of M-S bond energies on supported catalysts. Moreover, this hypothesis cannot easily explain the lower activity of $M(10\bar{1}0)$-based catalysts with respect to the $A(11\bar{2}0)$ crystal plane. Indeed, previous DFT calculations have suggested a similar surface structure for both crystal planes and both model catalysts exhibit active phase-support interactions of intermediate strength [20–22]. This interrogation calls for a deeper investigation of both surface structures. Nonetheless, our results confirm the determining role of the support on the activity, while implying that improved HDS activities are obtained through a compromise in the strength of metal-support interactions.

4.3 From the model system to the real catalyst

As previously pointed out, the results obtained with the model catalysts (α-Al_2O_3) can be transposed for the traditional support (γ-Al_2O_3) by comparison of surface sites. The studies carried out by Bara et al. [20,21] first proposed a relationship between α- and γ-Al_2O_3 surface structures [22]: the $R(1\bar{1}02)$ α-Al_2O_3 plane can be used as a surrogate for the predominant (110) γ-Al_2O_3 facet, the C(0001) α-Al_2O_3 plane can model the (111) γ-Al_2O_3 facet while the $A(11\bar{2}0)$ and $M(10\bar{1}0)$ α-Al_2O_3 planes expose surface OH groups that are reminiscent of those on the (111) and (100) γ-Al_2O_3 facets.

Based on our results and the proposed α/γ analogy, we may assign the surface-dependent catalytic conversions of Fig. 14 to specific surface facets of γ-Al_2O_3 (Fig. 16). The highest catalytic activity may then be associated to the (100) plane of γ-Al_2O_3 and the lowest activity to the (111) γ-Al_2O_3 plane modeled by the C(0001) surface. These results suggest that a porous γ-Al_2O_3 support especially designed to exhibit (100) sites would probably have positive effects on the HDS activity with respect to traditional catalysts with un-engineered supports.

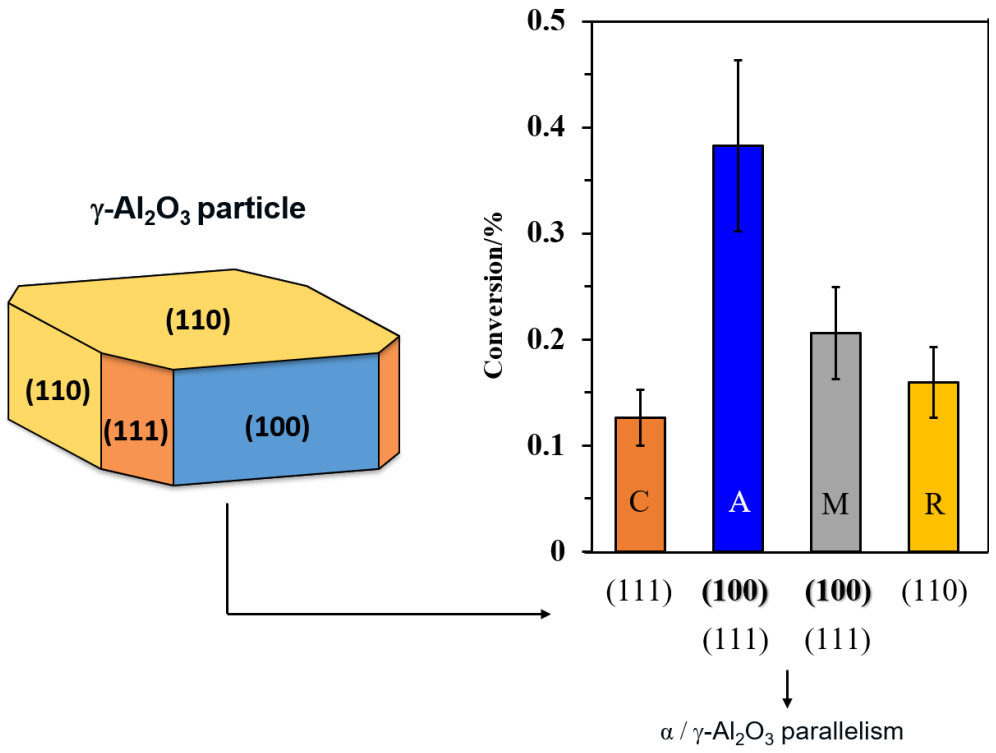

Figure 16. Schematic representation of the surface-dependent catalytic activity in terms of the crystal planes of γ-Al_2O_3 nanoparticle as reported by Digne et al. [66] by extrapolation from the results on the A$(11\bar{2}0)$, C(0001), M$(10\bar{1}0)$, and R$(1\bar{1}02)$ crystal planes of α-Al_2O_3.

5. Conclusions

Model Co-promoted Mo-based hydrotreating catalysts were studied and characterized under a surface science approach by using α-Al_2O_3 single crystals with four different orientations as model supports which allowed a better control of the speciation of surface sorption sites. CoMo model catalysts supported on α-Al_2O_3 planes A$(11\bar{2}0)$, C(0001), M$(10\bar{1}0)$, and R$(1\bar{1}02)$ were characterized in the oxide (after 450 °C calcination) and sulfide states in terms of cobalt and molybdenum speciation (XPS, XAS) and surface dispersion (AFM, TEM). Our results confirmed that the sulfidation degree (% MoS_2) is surface-dependent, the extent of the sulfidation being intimately related to the nature of the sorption sites and the resulting strength of metal/support interactions. It was found that the promotion extent (%Co in MoS_2) is also surface dependent below 400 °C, following the trend C(0001) > A$(11\bar{2}0)$, M$(10\bar{1}0)$ and R$(1\bar{1}02)$ which parallels the sulfidation degree. AFM and TEM also revealed a surface-dependent aggregation and stacking number of MoS_2 nanostructures. Both metal sulfidation and dispersion measurements confirmed the following trend in the strength of active phase-support interactions: R$(1\bar{1}02)$ > A$(11\bar{2}0)$, M$(10\bar{1}0)$ > C(0001).

Thiophene hydrodesulfurization showed that the highest conversion was reached on the A$(11\bar{2}0)$ plane while the other surfaces showed a substantially lower activity. It is proposed that the optimum in activity comes from a compromise between weak and strong active phase-support interactions, which modify the M-S bond energy of the CoMoS phase, leading to a surface-dependent volcano plot. Intermediate active-phase support interactions (A$(11\bar{2}0)$ plane) may lead to intermediate metal-sulfur bond energies in agreement with the Sabatier principle. Nonetheless, our current understanding of the A$(11\bar{2}0)$ and M$(10\bar{1}0)$ surface structures does not allow us to explain their different intrinsic activities.

The reductionist approach followed in this study may improve our understanding of the surface-dependent cobalt promotion and activity on industrial γ-Al_2O_3-based CoMo catalysts. The surface-dependent activity obtained on α-Al_2O_3 suggests that the most active surface sites are obtained on the (100) surface of γ-Al_2O_3 and engineering γ-Al_2O_3 in order to synthesize supports exhibiting primarily (100) surfaces would be a next step in order to bridge the gap between model and industrial catalysts.

Acknowledgements

We thank Dr. Cyril Thomas and Laurent Delannoy for their precious help in the development of the catalytic set-up. Sandra Casale and Anne-Lise Taleb are also acknowledged for their support on TEM experiments and data treating of TEM images respectively. We also thank Christophe Méthivier for his assistance in XPS data acquisition and analysis. We thank Valérie Briois for providing reference Co K-edge XANES spectra and Pascal Raybaud for fruitful discussions. Finally, we also acknowledge SOLEIL Synchrotron for provision of synchrotron radiation facilities (proposal 20190184), in particular Emiliano Fonda and Guillaume Alizon for their scientific and technical assistance throughout the experiences carried out at SAMBA beamline at SOLEIL.

References

[1] K.A. Rogers, Y. Zheng, Selective Deoxygenation of Biomass-Derived Bio-oils within Hydrogen-Modest Environments: A Review and New Insights, ChemSusChem. 9 (2016) 1750–1772.

[2] A. Gruia, Hydrotreating, in: Handb. Pet. Process., Springer Netherlands, Dordrecht, 2008: pp. 321–354.

[3] H. Toulhoat, P. Raybaud, Catalysis by transition metal sulphides : from molecular theory to industrial application, Editions TECHNIP, 2013.

[4] E. Payen, R. Hubaut, S. Kasztelan, O. Poulet, J. Grimblot, Morphology study of MoS_2-and WS_2-Based hydrotreating catalysts by high-resolution electron microscopy, J. Catal. 147 (1994) 123–132.

[5] S. Kasztelan, H. Toulhoat, J. Grimblot, J.P. Bonnelle, A geometrical model of the active phase of hydrotreating catalysts, Appl. Catal. 13 (1984) 127–159.

[6] C. Wivel, B.S. Clausen, R. Candia, S. Mørup, H. Topsøe, Mössbauer emission studies of calcined Co-$MoAl_2O_3$ catalysts: Catalytic significance of Co precursors, J. Catal. 87 (1984) 497–513.

[7] European Parliament, Directive 2009/30/EC of the European Parliament and of the Council, Off. J. Eur. Union. (2009) L140/88-L140/113.

[8] H. Topsøe, B.S. Clausen, R. Candia, C. Wivel, S. Mørup, In situ Mössbauer emission spectroscopy studies of unsupported and supported sulfided Co-Mo hydrodesulfurization catalysts: Evidence for and nature of a Co-Mo-S phase, J. Catal. 68 (1981) 433–452.

[9] On the catalytic significance of a Co-Mo-S phase in Co-$MoAl_2O_3$ hydrodesulfurization catalysts: Combined in situ Mössbauer emission spectroscopy and activity studies, J. Catal. 68 (1981) 453–463.

[10] B. Hinnemann, J. K. Nørskov, H. Topsøe, A Density Functional Study of the Chemical Differences between Type I and Type II MoS_2-Based Structures in Hydrotreating Catalysts, 109 (2004) 2245-2253.

[11] E. Krebs, B. Silvi, A. Daudin, P. Raybaud, A DFT study of the origin of the HDS/HydO selectivity on Co(Ni)MoS active phases, J. Catal. 260 (2008) 276–287.

[12] J. V Lauritsen, S. Helveg, E. Laegsgaard, I. Stensgaard, B.S. Clausen, H. Topsøe, F. Besenbacher, Atomic-Scale Structure of Co–Mo–S Nanoclustersin Hydrotreating Catalysts, J. Catal. 197 (2001) 1–5.

[13] J. V. Lauritsen, R.T. Vang, F. Besenbacher, From atom-resolved scanning tunneling microscopy (STM) studies to the design of new catalysts, Catal. Today. 111 (2006) 34–43.

[14] S. Helveg, J. V. Lauritsen, E. Lægsgaard, I. Stensgaard, J.K. Nørskov, B.S. Clausen, H. Topsøe, F. Besenbacher, Atomic-Scale Structure of Single-Layer MoS_2 Nanoclusters, Phys. Rev. Lett. 84 (2000) 951–954.

[15] J.V. Lauritsen, M.V. Bollinger, E. Lægsgaard, K.W. Jacobsen, J.K. Nørskov, B.S. Clausen, H. Topsøe, F. Besenbacher, Atomic-scale insight into structure and morphology changes of MoS_2 nanoclusters in hydrotreating catalysts, J. Catal. 221 (2004) 510–522.

[16] J.C. Muijsers, T. Weber, R.M. Vanhardeveld, H.W. Zandbergen, J.W. Niemantsverdriet, Sulfidation Study of Molybdenum Oxide Using MoO_3/SiO_2/Si(100) Model Catalysts and Mo-IV3-Sulfur Cluster Compounds, J. Catal. 157 (1995) 698–705.

[17] Y. Sakashita, T. Yoneda, Orientation of MoS_2 Clusters Supported on Two Kinds of γ-Al_2O_3 Single Crystal Surfaces with Different Indices, J. Catal. 185 (1999) 487–495.

[18] Y. Sakashita, Effects of surface orientation and crystallinity of alumina supports on the microstructures of molybdenum oxides and sulfides, Surf. Sci. 489 (2001) 45–58.

[19] C. Bara, E. Devers, M. Digne, A.-F. Lamic-Humblot, G.D. Pirngruber, X. Carrier, Surface Science Approaches for the Preparation of Alumina-Supported Hydrotreating Catalysts, ChemCatChem. 7 (2015) 3422–3440.

[20] C. Bara, L. Plais, K. Larmier, E. Devers, M. Digne, A.-F. Lamic-Humblot, G.D. Pirngruber, X. Carrier, Aqueous-Phase Preparation of Model HDS Catalysts on Planar Alumina Substrates: Support Effect on Mo Adsorption and Sulfidation, J. Am. Chem. Soc. 137 (2015) 15915–15928.

[21] C. Bara, A.F. Lamic-Humblot, E. Fonda, A.S. Gay, A.L. Taleb, E. Devers, M. Digne, G.D. Pirngruber, X. Carrier, Surface-dependent sulfidation and orientation of MoS_2 slabs on alumina-supported model hydrodesulfurization catalysts, J. Catal. 344 (2016) 591–605.

[22] R.A. Garcia de Castro, J. Bertrand, B. Rigaud, E. Devers, M. Digne, A.-F. Lamic-Humblot, G. Pirngruber, X. Carrier, Surface-dependent activation of model α-Al_2O_3-supported P-doped hydrotreating catalysts prepared by spin coating, Chem. – A Eur. J. (2020) chem.202001882.

[23] R. Prins, On the structure of γ-Al_2O_3, J. Catal. 392 (2020) 336–346.

[24] A. Tougerti, C. Méthivier, S. Cristol, F. Tielens, M. Che, X. Carrier, Structure of clean and hydrated α-Al_2O_3 ($1\bar{1}02$) surfaces: implication on surface charge, Phys. Chem. Chem. Phys. 13 (2011) 6531.

[25] A.D. Gandubert, C. Legens, D. Guillaume, S. Rebours, E. Payen, X-ray Photoelectron Spectroscopy Surface Quantification of Sulfided CoMoP Catalysts – Relation Between Activity and Promoted Sites – Part I: Influence of the Co/Mo Ratio, Oil Gas Sci. Technol. - Rev. l'IFP. 62 (2007) 79–89.

[26] A.D. Gandubert, C. Legens, D. Guillaume, E. Payen, X-ray photoelectron spectroscopy surface quantification of sulfided CoMoP catalysts. Relation between activity and promoted sites. Part II: Influence of the sulfidation temperature, Surf. Interface Anal. 38 (2006) 206–209.

[27] Casa software Ltd, CasaXPS Manual, (2009) 342.

[28] S.N. Towle, G.E. Brown, G.A. Parks, Sorption of Co(II) on metal oxide surfaces: I. Identification of specific binding sites of Co(II) on (110) and (001) surfaces of TiO_2 (rutile) by grazing-incidence XAFS spectroscopy, J. Colloid Interface Sci. 217 (1999) 299–311.

[29] S. Tanuma, C.J. Powell, D.R. Penn, Calculations of electron inelastic mean free paths. V. Data for 14 organic compounds over the 50–2000 eV range, Surf. Interface Anal. 21 (1994) 165–176.

[30] C.A. Schneider, W.S. Rasband, K.W. Eliceiri, NIH Image to ImageJ: 25 years of image analysis., Nat. Methods. 9 (2012) 671–5.

[31] A. Calisti, C. Mossé, S. Ferri. UVX 2010 - 10e Colloque sur les Sources Cohérentes et Incohérentes UV, VUV et X; Applications et Développements Récents. EDP Sciences (2011).

[32] B. Ravel, M. Newville, ATHENA, ARTEMIS, HEPHAESTUS: Data analysis for X-ray absorption spectroscopy using IFEFFIT, J. Synchrotron Radiat., International Union of Crystallography, 12 (2005) 537–541.

[33] L. Plais, C. Lancelot, C. Lamonier, E. Payen, V. Briois, First in situ temperature quantification of CoMoS species upon gas sulfidation enabled by new insight on cobalt sulfide formation, Catal. Today. (2020).

[34] A.J. Andreatch, R. Feinland, Continuous Trace Hydrocarbon Analysis by Flame Ionization, Anal. Chem. 32 (1960) 1021–1024.

[35] V. León, A simplified Kerkhof-Moulijn model for dispersion quantification from XPS atomic concentrations, Surf. Sci. 339 (1995) L931–L934.

[36] P.J. Eng, T.P. Trainor, G.E.B. Brown, G.A. Waychunas, M. Newville, S.R. Sutton, M.L. Rivers, Structure of the hydrated alpha-Al_2O_3 (0001) surface, Science. 288 (2000) 1029–33.

[37] A. Dandapat, G. De, Host-mediated synthesis of cobalt aluminate/γ-alumina nanoflakes: A dispersible composite pigment with high catalytic activities, ACS Appl. Mater. Interfaces. 4 (2012) 228–234.

[38] J.A. Rodriguez, S. Chaturvedi, J.C. Hanson, A. Albornoz, J.L. Brito, Electronic properties and phase transformations in $CoMoO_4$ and $NiMoO_4$: XANES and time-resolved synchrotron XRD studies, J. Phys. Chem. B. 102 (1998) 1347–1355.

[39] Y. Okamoto, H. Nakano, T. Shimokawa, T. Imanaka, S. Teranishi, Stabilization effect of Co for Mo phase in CoMo Al_2O_3 hydrodesulfurization catalysts studied with X-Ray photoelectron spectroscopy, J. Catal. 50 (1977) 447–454.

[40] T. Seiyama, K. Tanabe, New horizons in catalysis: proceedings of the 7th International Congress on Catalysis, Tokyo, 30 June-4 July 1980, (1981).

[41] J. Kibsgaard, Atomic-scale investigation of MoS_2-based hydrotreating model catalysts. A scanning tunneling microscopy study, Ph.D. Dissertation, Aarhus University, (2008).

[42] G. Berhault, M. Perez De la Rosa, A. Mehta, M.J. Yácaman, R.R. Chianelli, The single-layered morphology of supported MoS_2-based catalysts-The role of the cobalt promoter and its effects in the hydrodesulfurization of dibenzothiophene, Appl. Catal. A Gen. 345 (2008) 80–88.

[43] D. Gao, A. Duan, X. Zhang, Z. Zhao, H. E, Y. Qin, C. Xu, Synthesis of CoMo catalysts supported on EMT/FAU intergrowth zeolites with different morphologies and their hydro-upgrading performances for FCC gasoline, Chem. Eng. J. 270 (2015) 176–186.

[44] E. Krebs, B. Silvi, P. Raybaud, Mixed sites and promoter segregation: A DFT study of the manifestation of Le Chatelier's principle for the Co(Ni)MoS active phase in reaction conditions, Catal. Today. 130 (2008) 160–169.

[45] B. Baubet, M. Girleanu, A.-S. Gay, A.-L. Taleb, M. Moreaud, F. Wahl, V. Delattre, E. Devers, A. Hugon, O. Ersen, P. Afanasiev, P. Raybaud, Quantitative Two-Dimensional (2D) Morphology–Selectivity Relationship of CoMoS Nanolayers: A Combined High-Resolution High-Angle Annular Dark Field Scanning Transmission Electron Microscopy (HR HAADF-STEM) and Density Functional Theory (DFT) Study, ACS Catal. 6 (2016) 1081–1092.

[46] M. Breysse, J.L. Portefaix, M. Vrinat, Support effects on hydrotreating catalysts, Catufysis Today Elsevier Sci. Publ. B.V. 10 (1991) 489–505.

[47] G. Kishan, L. Coulier, J.A. van Veen, J. Niemantsverdriet, Promoting Synergy in CoW Sulfide Hydrotreating Catalysts by Chelating Agents, J. Catal. 200 (2001) 194–196.

[48] G. Kishan, J.A.R. van Veen, J.W. Niemantsverdriet, Realistic Surface Science Models of Hydrodesulfurization Catalysts on Planar Thin-Film Supports: The Role of Chelating Agents in the Preparation of CoW/SiO_2 catalysts, Top. Catal. 29 (2004) 103–110.

[49] D.L. Sullivan, J.G. Ekerdt, Mechanisms of Thiophene Hydrodesulfurization on Model Molybdenum Catalysts, J. Catal. 178 (1998) 226–233.

[50] J. Ramírez, P. Castillo, L. Cedeño, R. Cuevas, M. Castillo, J. Palacios, A. López-Agudo, Effect of boron addition on the activity and selectivity of hydrotreating CoMo/Al_2O_3 catalysts, Appl. Catal. A Gen. 132 (1995) 317–334.

[51] S. Kolboe, Catalytic hydrodesulfurization of thiophene. VII. Comparison between thiophene, tetrahydrothiophene, and n-butanethiol, Can. J. Chem. 47 (1969) 352–355.

[52] A.C. Sorensen, B.L. Fuller, A.G. Eklund, C.C. Landry, Mo-doped mesoporous silica for thiophene hydrodesulfurization: Comparison of materials and methods, Chem. Mater. 16 (2004) 2157–2164.

[53] E.J. Markel, G.L. Schrader, N.N. Sauer, R.J. Angelici, Thiophene, 2,3- and 2,5-dihydrothiophene, and tetrahydrothiophene hydrodesulfurization on Mo and Re γ-Al_2O_3 catalysts, J. Catal. 116 (1989) 11–22.

[54] M. Zdražil, Recent advances in catalysis over sulphides, Catal. Today. 3 (1988) 269–365.

[55] C. Arrouvel, M. Breysse, H. Toulhoat, P. Raybaud, A density functional theory comparison of anatase (TiO_2)- and γ-Al_2O_3-supported MoS_2 catalysts, J. Catal. 232 (2005) 161–178.

[56] R.G. Leliveld, A.J. van Dillen, J.W. Geus, D.C. Koningsberger, The sulfidation of γ-alumina and titania supported (cobalt)molybdenum oxide catalysts monitored by EXAFS, J. Catal. 171 (1997) 115–129.

[57] E. Diemann, T. Weber, A. Müller, Modeling the thiophene HDS reaction on a molecular level, J. Catal. 148 (1994) 288–303.

[58] L. van Haandel, G.M. Bremmer, E.J.M. Hensen, T. Weber, Influence of sulfiding agent and pressure on structure and performance of CoMo/Al_2O_3 hydrodesulfurization catalysts, J. Catal. 342 (2016) 27–39.

[59] C. Lesage, E. Devers, C. Legens, G. Fernandes, O. Roudenko, V. Briois, High pressure cell for edge jumping X-ray absorption spectroscopy: Applications to industrial liquid sulfidation of hydrotreatment catalysts, Catal. Today. 336 (2019) 63–73.

[60] D. Laurenti, B. Phung-Ngoc, C. Roukoss, E. Devers, K. Marchand, L. Massin, L. Lemaitre, C. Legens, A.-A. Quoineaud, M. Vrinat, Intrinsic potential of alumina-supported CoMo catalysts in HDS: Comparison between γc, γT, and δ-alumina, J. Catal. 297 (2013) 165–175.

[61] E. Dominguez Garcia, J. Chen, E. Oliviero, L. Oliviero, F. Maugé, New insight into the support effect on HDS catalysts: evidence for the role of Mo-support interaction on the MoS_2 slab morphology, Appl. Catal. B Environ. 260 (2020) 117975.

[62] A.S. Walton, J. V. Lauritsen, H. Topsøe, F. Besenbacher, MoS2 nanoparticle morphologies in hydrodesulfurization catalysis studied by scanning tunneling microscopy, J. Catal. 308 (2013) 306–318.

[63] H. Toulhoat, P. Raybaud, Kinetic interpretation of catalytic activity patterns based on theoretical chemical descriptors, J. Catal., (2003) 63–72.

[64] H. Toulhoat, P. Raybaud, Prediction of optimal catalysts for a given chemical reaction, Catal. Sci. Technol. 10 (2020) 2069–2081.

[65] D. Costa, C. Arrouvel, M. Breysse, H. Toulhoat, P. Raybaud, Edge wetting effects of γ-Al_2O_3 and anatase-TiO_2 supports by MoS_2 and CoMoS active phases: A DFT study, J. Catal. 246 (2007) 325–343.

[66] M. Digne, P. Sautet, P. Raybaud, P. Euzen, H. Toulhoat, Use of DFT to achieve a rational understanding of acid–basic properties of γ-alumina surfaces, J. Catal. 226 (2004) 54–68.